Shape change of tensegrity structures
design and control

van de Wijdeven, J.J.M.

Award date:
2004

Shape Change of Tensegrity Structures: Design and Control

J.J.M. van de Wijdeven

DCT 2004.02

Master's thesis

Coach(es): dr.ir. B. de Jager

Supervisor: prof. dr. ir. M. Steinbuch

Technische Universiteit Eindhoven
Department Mechanical Engineering
Dynamics and Control Technology Group

Eindhoven, January 2004

Abstract

Tensegrity structures are structures built up from bars and tendons, where bars are placed discontinuous in a continuous network of tendons. While tendons can only handle tensile forces, bars can be subjected to both tensile and compressive forces. Integrity (stability) of the tensegrity structure is obtained through pre-stress of the tendons. The focus of this report is on Class 1 tensegrity structures, which means that bars are only attached to tendons, not to other bars.

The first goal of the research is to develop a method for generating reference trajectories for shape changes of an arbitrary Class 1 tensegrity structure. The second goal is to find a controller that focusses on tracking of a given shape trajectory, while accounting for the integrity of the tensegrity structure.
To reach the goals, first kinematic relations, nonlinear dynamics and statics are derived. Singularities in the dynamics are omitted by introducing Euler parameters. Dynamics related to restrictions in the structure are removed from the final dynamics. The analysis of the statics, used for integrity checks, has been done with and without the influence of gravity.
After gathering the different constraints related to shape changes, an optimization algorithm for generating reference trajectories is presented. The constraints include singularity avoidance, collision detection, and issues related to geometry and element forces.
After several control strategies are studied, the $\mathcal{H}_2$ control strategy is selected for tracking of the shape changes. For design of the controller, a linear model of the nonlinear dynamics is required. The procedure for linearization is presented. Issues, related to the design of an $\mathcal{H}_2$ controller, are discussed.
As an example, a reference trajectory and corresponding controller are designed for a two dimensional Class 1 tensegrity structure. Results illustrate the success of the reference trajectory generator. When the reference trajectory is merely used for a feedforward signal, poorly damped structural vibrations are visible in measurements and tendons sometimes go slack, due to lack of tension. Including the $\mathcal{H}_2$ controller in the closed loop system, it is shown that tracking errors are reduced, vibrations are suppressed and tension in tendons is preserved.

Samenvatting

Tensegrity structures zijn structuren, opgebouwd uit balken en kabels. De balken zijn discontinu geplaatst in een continu netwerk van kabels. Terwijl kabels alleen trekkrachten kunnen verwerken, kunnen balken belast worden op zowel trek- als drukkrachten. Door kabels voor te spannen, kan de structuur zijn integriteit (stabiliteit) behouden. In dit verslag is de aandacht gericht op Class 1 tensegrity structures, wat inhoudt dat balken alleen verbonden zijn met kabels en niet met andere balken.

Het eerste doel van het onderzoek is, om een methode te ontwikkelen voor het genereren van referentietrajectories voor vormveranderingen van een willekeurige Class 1 tensegrity structure. Het tweede doel is het vinden van een regelaar, die gericht is op het volgen van de vormverandering, maar daarnaast ook rekening houdt met de integriteit van de tensegrity structure.
Om deze doelen te bereiken, zijn eerst kinematische vergelijkingen, een niet-lineair dynamisch model en de statica van een willekeurige Class 1 tensegrity structure afgeleid. Singulariteiten in de dynamica worden vermeden door het introduceren van Euler parameters. Dynamica die gerelateerd is aan restricties, wordt uit het niet-lineaire model verwijderd. De analyse van de statica, die nodig is voor het controleren van de integriteit, is uitgewerkt voor situaties waarbij zwaartekracht wel en geen rol speelt.
Nadat de verschillende beperkingen, gerelateerd aan de vormveranderingen, verzameld zijn, wordt een optimalisatie-algoritme gepresenteerd voor het genereren van een referentietrajectorie. De beperkingen zijn onder te verdelen in het ontwijken van singulariteiten in de structuur, het detecteren van botsingen tussen elementen en beperkingen die verband houden met de geometrie van en het krachtenspel in de structuur.
Na bespreking van een aantal regelstrategiëen, wordt gekozen om de vormveranderingen te regelen met een $\mathcal{H}_2$ regelaar. Aangezien de regelaar gebaseerd is op een lineair systeem, wordt de niet-lineaire dynamica eerst gelineariseerd. Vervolgens worden de verschillende aspecten, behorende bij het regelaarontwerp, besproken.
Ter illustratie wordt een referentietrajectorie en regelaar ontworpen voor een twee dimensionale Class 1 tensegrity structure. Resultaten geven aan dat de referentietrajectorie generator goed functioneert. Als de referentietrajectorie alleen wordt gebruikt als feedforward signaal, zijn slecht uitdempende vibraties in de metingen zichtbaar en komen kabels soms slap te hangen. Door toevoeging van de $\mathcal{H}_2$ regelaar in het systeem, worden vibraties sterk verminderd, volgfouten verkleind en behouden de kabels hun voorspanning.

List of symbols

Notations

Notation	Description
$(\cdot)_t$	$(\cdot)$ for tendons
$(\cdot)_b$	$(\cdot)$ for bars
$\|\| \cdot \|\|$	Euclidean norm of $(\cdot)$
$(\cdot)^T$	Transpose of $(\cdot)$
$\dot{(\cdot)}$	Time derivative of $(\cdot)$
$(\cdot)_{ref}$	Reference variable $(\cdot)$

Symbols

Symbol	Description
A_b, A_t	Cross sectional area
C_b, C_t	Topology matrix
C_{map}	Permutation matrix for nodal positions
c_{1i}, c_{2i}	Vectors from center of mass to ends of bar i
d_{damp}	Damping coefficient of the tendons
E	Young's modulus for elasticity
e_0, e_1, e_2, e_3	Euler parameters
$\underline{\vec{e}}^{\,0}$	Global frame
$\underline{\vec{e}}^{\,1}$	Local bar frame
F_b	Resulting force vector, working on the center of mass of a bar
F_n	Resulting force vector, working on a node
F_t	Force vector of a tendon
G	Gravity vector
I	Identity matrix / second moment of area of a bar
$\mathbb{J}$	Inertia tensor of a bar
L_b, L_t	Element length

continued on the next page –

– *continued from previous page*

Symbol	Description
L_{dist}	Distance between two elements
L_{t_0}	Rest length of tendons
M_b	Resulting momentum vector, working on the center of mass of a bar
M_m, M_{m2}	Mass matrices
m	Mass of a bar
n_b	Number of bars in the tensegrity structure
n_t	Number of tendons in the tensegrity structure
p	Nodal position vector
q	Generalized coordinate vector
R	Rotation matrix
r	Position vector of center of mass of a bar
r_1, r_2	Outer radii of elements
S_b, S_t	Connectivity matrix
t	Element vector
t_{dist}	Distance vector between two elements
w	External load / disturbance
θ, φ	Orientation of bars in 3D tensegrity structures
κ	Safety factor
σ	Singular value
σ_{yield}	Yield stress
ϕ	Orientation of bars in 2D tensegrity structures
ω	Angular velocity vector

Contents

Chapter 1

Introduction

Tensegrity structures are structures build up from bars and tendons (strings), first created by Kenneth Snelson [1]. The bars are floating discontinuously in a continuous network of tendons, with the tendons attached to the bars. While tendons can only handle tensile forces, bars can be subjected to both tensile and compressive forces. Only when the configuration is in stable equilibrium, one may speak of a tensegrity structure.
The word "tensegrity" is coined from the words "tension" and "integrity", with the latter indicating the stable equilibrium or integrity of the structure. A simple example of a tensegrity structure is presented in Figure 1.1; the thick lines are bars, the thin lines are tendons.

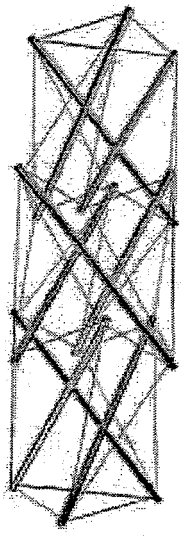

Figure 1.1: Class 1 tensegrity structure [2]

In a Class 1 tensegrity structure the bars only connect to tendons, while in a Class 2 tensegrity structure the ends of two bars can be connected, together with a number of tendons, in

a single joint. In both cases bending moments on elements are not allowed in the structure, demanding that the joints do not impart torques. This demand can be met by using, e.g., ball joints. For Class 1 tensegrity structures, ball joints are not needed when tendons are non-stiff for bending. The result of absence of bending moments is, that in a tensegrity structure forces only work axially on the elements and therefor make the elements more efficient to carry loads. This efficiency makes it possible to make stiff, yet relatively light structures. In applications where mass is very important, e.g., space applications, this mass to stiffness ratio is a huge benefit. Multiple studies on stiffness have been conducted. For example, in [3] not only an extended introduction to tensegrity structures is presented, stiffness calculations on numerous tensegrity structures are done. In [4] and [5] the focus is on optimizing the stiffness of a tensegrity structure.
A tensegrity structure is a redundant structure. This means that there are more tendons present in the structure than is needed to have a determined system. The benefit of this redundancy is that the tendons can be under tension, while the shape of the tensegrity structure is maintained. Besides geometry and material properties of the elements, tension in the tendons influences the stiffness of the whole structure. If the tension in the tendons is increased, the stiffness of the complete structure is increased. This can be done passively by adjusting the tension in the tendons during the construction of the tensegrity structure, or actively through actuators attached to or build in to the tendons or bars.
To obtain an increase in tension, the difference between the rest length (unstressed) and the stressed length of a tendon must be increased. In [5] examples of possible actuators have been presented: a shape memory alloy reacting on changes in temperature, or linear or rotary motors. Although extensible bars are also mentioned as actuators, in this report bars are considered to be passive elements, meaning that their lengths cannot be actively altered.

The possibility to actively change the rest length of tendons makes it possible to alter the shape of the complete tensegrity structure, or to correct for external disturbances in order to maintain a desired shape. This aspect makes tensegrity structures an interesting alternative for current structures used for space applications, e.g., deployable antennas or radio telescopes or in the medical field in the sense of minimal invasive surgery.
In [6] variations in tendon length are used for deployment of a tensegrity structure. The rest length of the tendons in the tensegrity structure is derived from time optimal control in which a shape dependent parameter is used. No further control is applied to correct for dynamic effects during and after the deployment. In [7] a time optimal path is determined for kinematically invertible tensegrity structures, together with a feedback linearization controller. The controller includes saturation avoidance in the tendons, i.e., making sure the tendons do not go slack or snap due to forces greater than the yield force. In [8] several control strategies for path tracking of a tensegrity structure are explored, such as LQG control, neural networks and gain scheduling control. Neural networks are used to approximate the inverse kinematics. This resulted in a trajectory for the tensegrity structure to follow, but no feedback control is used to guarantee the tracking. With LQG and Gain Scheduling Control in [8], no serious attention is paid to the design of a reference trajectory. In [9] the control strategy consists of two H_∞ controllers, with switching between controllers during the shape change.

Although the topics of path or reference generation, i.e., the shape change of a tensegrity structure, and control of a tensegrity structure during and after shape changes are discussed in the literature of the previous paragraph, there is still a lot to study in these fields. The trajectories determined in the above mentioned literature are only valid for specific cases. For an arbitrary tensegrity structure no algorithms or methods for path generation are available.
A small number of control strategies have been applied to tensegrity structures. There are however doubts about the practical usefulness of some controllers. Therefor it is desired to look for possible new control strategies for tracking of a reference trajectory.

The focus of this research is chosen to be on shape changes of arbitrary Class 1 tensegrity structures. The goal is twofold and defined as:

- *Develop a method for generating a reference trajectory for shape changes of an arbitrary Class 1 tensegrity structure.*
- *Find a control strategy for an arbitrary Class 1 tensegrity structure that focusses on tracking of a given shape trajectory, while accounting for the integrity of the tensegrity structure.*

Though derivation of the descriptions for kinematics, dynamics and statics is not a specific goal of the research, it will be treated extensively. The descriptions will be used as tools for the development of the reference trajectory generator and design of the controller.
Statics are used to obtain information about the integrity of the tensegrity structure. In [4] static equations are derived for situations where the influence of gravity is absent.
Dynamic models make it possible to study system properties, e.g., eigenfrequencies and damping from linearizations of the dynamics. Furthermore, the dynamics can be used to obtain time responses of a tensegrity structure. In [8], the dynamics for a Class 1 tensegrity structure are derived including Lagrange multipliers for the handling of restrictions, e.g., joints. In [9], restrictions are eliminated from the dynamics by removing the unknown reaction forces from the equations of motion. Both [8] and [9] use Euler angles or Tait-Bryant angles to describe the dynamic equations, which can cause singularities.

In Chapter 2, first kinematic relations, nonlinear dynamics and statics are derived. Singularities, present in the dynamics of [8] and [9], will be omitted by introducing Euler parameters. As in [9], dynamics related to restrictions in the structure, will be removed from the final dynamics. The analysis of the statics, used for integrity checks, is done with and without the influence of gravity.
In Chapter 3 an optimization algorithm for generating reference trajectories is derived. Constraints related to shape changes are defined. Different optimization objectives and optimization variables will be discussed.
In order to guarantee good tracking of a tensegrity structure to a reference trajectory, a feedback controller is needed. In Chapter 4 several control strategies are studied and one control strategy is selected for tracking of the shape changes. For design of the feedback

controller, a linear model of the nonlinear dynamics is used. The procedure for linearization is presented. Issues, related to the design of the feedback controller, will be discussed.
In Chapter 5, reference trajectory generation and control design will be applied to a two dimensional Class 1 tensegrity structure. Results from the reference trajectory generator and time responses of the tensegrity structure are presented. After the controller is designed, analysis of the closed loop system is done and time responses of the closed loop system are given.
Finally, in Chapter 6 conclusions are presented and recommendations for further research are given.

Chapter 2

Class 1 tensegrity structures

In this Chapter different descriptions for Class 1 tensegrity structures are derived: kinematics, dynamics and statics. The dynamics of multi-body systems with bars and tendons can be very complex. To simplify the dynamics, in Section 2.1 a number of assumptions is made. Nodal positions, generalized coordinates and the kinematics are presented in Section 2.2. Using multi-body dynamics and the kinematic relations, the dynamics of a Class 1 tensegrity structure is derived in Section 2.3. Finally, in Section 2.4 the statics of a tensegrity structure, important for checking the integrity of the structure, is presented.

2.1 Assumptions

To avoid too much complexity in the dynamic models of a tensegrity structure, a number of assumptions is made. These assumptions relate to material properties and geometric properties of the elements in a tensegrity structure:

- The bars are considered to be rigid. This means no deformations like buckling or length variations will be modelled in the dynamics. Although this is a huge assumption, it does make it possible to use classical multi-body dynamic theory to model the tensegrity structure.
- Without loss of generality the bars are assumed to be round and symmetric and the centers of mass are positioned at the center of the bars.
- The tendons have zero mass. Again this is a huge assumption, but it makes the modelling of the dynamics of a tensegrity structure a lot easier. The tendons can now be modelled as a one-sided spring. The one-sidedness corresponds to the fact that tendons can only cope with tensile forces and not with compressive forces.

  When looking at the situation where the tendons do have mass, a lot of extra bodies with varying length are introduced to the system. They each have their own inertia and gravitational influences, increasing the complexity enormously.
- When a tensile force works on the tendon, the tendon is modelled as a *linear* spring. When tendons are made of steel, this is a correct assumption. It is also possible to use

other materials with their own elastic properties. The linear elastic spring however is the easiest to model and therefor chosen.

- Tendons have a constant cross sectional area, independent of the forces that work on the tendons. For stiff materials this is a safe assumption, since the elongations of a tendon are very small compared to its rest length. Stiffness will thus not change when a tendon is subject to a force (assuming no changes in rest length of the tendon).
- When a tensegrity structure is connected to the fixed world by joints, only one end of a bar is allowed to be connected to this world. Again this makes the modelling of the dynamics a lot easier, while no stringent constraints on the design of a tensegrity structure are introduced.
- Forces from tendons and external forces only work on the ends of the bars (nodes). A resulting force will not result in axial rotation of the corresponding bar, i.e., works on the center of a node.
- There is no friction present in joints between elements, or between elements and the fixed world. This again results in a simplification of the dynamic model.

2.2 Kinematics

For a description of the kinematic relations, first the geometry and topology of the tensegrity structure must be properly defined. In Section 2.2.1 and 2.2.2 two geometric presentations are introduced: nodal positions and generalized coordinates. The kinematic relations between the two geometric presentations as well as the kinematics between nodal positions and length of elements is presented in Section 2.2.3.
Geometric presentations and kinematic relations for both 2D and 3D tensegrity structures are derived in this Section. The advantage of the study of 2D tensegrity structures is, that often the structure is easier to visualize than a 3D tensegrity structures, while much of the applied theory can remain the same.

2.2.1 Nodal positions

One way to define a tensegrity structure is by specifying the nodal positions. Nodal positions are the coordinates of the ends of the bars and there are thus $2n_b$ nodes, with n_b the number of bars. Dependent on the dimension of the structure there are two or three coordinates, x_i, y_i (and z_i) that describe the position $p_i = \begin{bmatrix} x_i & y_i & (z_i) \end{bmatrix}^T$ of node i. Figure 2.1 presents the nodal positions of one bar. When all $2n_b$ nodes in the structure are gathered, they can be described by a vector p, with $p = \begin{bmatrix} p_1^T & p_2^T & \dots & p_{2n_b}^T \end{bmatrix}^T$.
In a tensegrity structure the endpoints of an element (bar or tendon) connect two nodes. When all connections are gathered, a connectivity matrix S is formed. The matrix S can be divided into two sections: $S = [S_t; S_b]$. The first section S_t contains the connections made up by the tendons, the second section S_b those made up by bars.

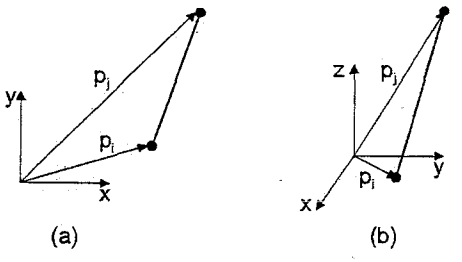

Figure 2.1: Nodal positions in a tensegrity structure, a) 2D b) 3D

Combining the geometry, described in vector p and the topology, described in S, the structure of the tensegrity structure is defined.

2.2.2 Generalized coordinates

A generalized coordinate q_i describes the position and orientation of the center of mass of a body with respect to an observer. For a 2D situation, the generalized coordinates contain two positions and one angle, $q_i = \begin{bmatrix} q_{x_i} & q_{y_i} & \phi_i \end{bmatrix}^T$, with $-\pi/2 \leq \phi_i \leq \pi/2$. The 2D generalized coordinates are illustrated by Figure 2.2(a).
In a 3D situation a rigid body has six Degrees Of Freedom (DOFs): three translations and three rotations. For a 3D tensegrity structure the rotation in the axial direction of a bar is neglected, due to the absence of a momentum in that direction. Therefor generalized coordinates only have five DOF per bar: three translations and two rotations.
A rotation in 3D can be expressed in Euler Angles or Tait-Bryant Angles [10], although there are many other expressions possible. These coordinates describe the sequence of rotations around the local axes. Euler Angles and Tait-Bryant Angles only differ in the choice which axis is used for the third rotation. This means that in the case of tensegrity structures it does not make a difference which coordinates are used.
The choice has been made to first rotate around the local z-axis by an angle θ ($-\pi/2 \leq \theta \leq \pi/2$) and subsequently rotate around the local y-axis with an angle φ, with $0 \leq \varphi \leq 2\pi$. The generalized coordinates for a 3D element are $q_i = \begin{bmatrix} q_{x_i} & q_{y_i} & q_{z_i} & \theta_i & \varphi_i \end{bmatrix}^T$. In Figure 2.2(b) the generalized coordinates for one 3D element are presented. Gathering the generalized coordinates of all n_b bars results in the vector $q = \begin{bmatrix} q_1^T & q_2^T & \dots & q_{n_b}^T \end{bmatrix}^T$.
A benefit of generalized coordinates over nodal positions is, that they describe the geometry of a structure with the minimum DOFs per bar (five), while nodal positions use six DOFs. This is under the assumption that the length of the bars are constant and known.
For a full description of the structure of a tensegrity structure, the generalized coordinates, the topology and the length of the bars are required. The positions of the center of mass of the bars are assumed to be known (see 2.1).

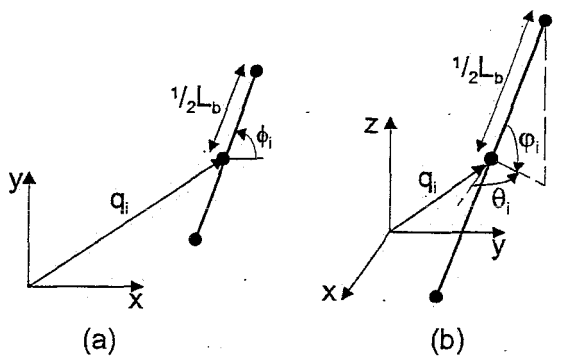

Figure 2.2: Generalized coordinates in a tensegrity structure, a) 2D b) 3D

2.2.3 Kinematic relations

For the static situation, three kinematic relations, or mappings, are of importance. These mappings appear between length of elements, nodal positions and generalized coordinates. In Figure 2.3 the different mappings are presented schematically. In the different subsections in this section, it will become clear whether a mapping is unique or not.

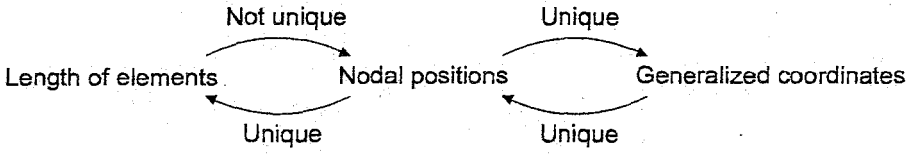

Figure 2.3: Mappings between different geometric presentations

The kinematic relations for 2D and 3D tensegrity structures will be discussed separately.

2D Kinematic Relations

The kinematic relations between nodal positions and generalized coordinates are straight forward. The relations are given in Eq.(2.1) and Eq.(2.2), which are directly derived from Figure 2.1(a) and 2.2(a).

$$
\begin{aligned}
q_i &= f_{qp}(p_i) \\
\begin{bmatrix} q_{x_i} \\ q_{y_i} \\ \phi_i \end{bmatrix} &= \begin{bmatrix} \frac{p_{x_i}+p_{x_j}}{2} \\ \frac{p_{y_i}+p_{y_j}}{2} \\ \sin^{-1}\left(\frac{p_{y_j}-p_{y_i}}{L_b}\right) \end{bmatrix}
\end{aligned}
\tag{2.1}
$$

$$
\begin{aligned}
p_i &= f_{pq}(q_i) \\
\begin{bmatrix} p_{x_i} \\ p_{y_i} \\ p_{x_j} \\ p_{y_j} \end{bmatrix} &= \begin{bmatrix} q_{x_i} - \frac{Lb}{2}\cos(\phi_i) \\ q_{y_i} - \frac{Lb}{2}\sin(\phi_i) \\ q_{x_i} + \frac{Lb}{2}\cos(\phi_i) \\ q_{y_i} + \frac{Lb}{2}\sin(\phi_i) \end{bmatrix}
\end{aligned} \tag{2.2}
$$

These mappings use the information about the position of the centers of mass of the bars. With this knowledge, the mapping from q to p is unique. For a unique mapping from p to q bounds on the value of ϕ_i are needed. In 2.2.2 these bounds have already been presented, namely $-\pi/2 \leq \phi_i \leq \pi/2$.

For the kinematic relation between nodal positions and the length of an element a vector representation of the element is useful. The element vector t_i is computed as the difference between the positions of the nodes it is connected to, with the convention that the vector points in the up/right direction.
In Eq.(2.3) the element vector t is defined, with n_t+n_b the total number of elements. Vector p contains the nodal positions and C is the topology matrix whose i,j block is I_2 when the element i ends at the j^{th} node, and $-I_2$ when it starts at the j^{th} node. Otherwise the topology matrix is filled with 0_2 [4]. Furthermore C can be divided into $C = [C_t; C_b]$, where C_t contains the topology for the tendons and C_b for the bars.

$$
t = Cp, \quad \text{with } t_i = \begin{bmatrix} t_{x_i} & t_{y_i} \end{bmatrix}^T \text{ and } t = \begin{bmatrix} t_1^T & t_2^T & \dots & t_{n_t}^T & t_{n_t+1}^T & \cdots & t_{n_t+n_b}^T \end{bmatrix}^T \tag{2.3}
$$

With the element vector defined, it is a small step to find the length of the elements, since it is only the Euclidean norm of t_i. Eq.(2.4) and Eq.(2.5) present the results. C_i contains the two rows that correspond to the i^{th} element.

$$
\begin{aligned}
L_{t_i} &= f_{L_i p}(p) \\
L_{t_i} &= ||t_i|| = \left(t_i^T t_i\right)^{1/2} = \left(p^T C_i^T C_i p\right)^{1/2} \quad \text{for } i = 1, 2, \dots, n_t && (2.4) \\
L_{b_i} &= ||t_i|| \quad \text{for } i = n_t+1, n_t+2, \dots, n_t+n_b && (2.5)
\end{aligned}
$$

The kinematic relation from the length of the elements to nodal positions is more complicated. To find the nodal positions, quadratic equations must be solved. These quadratic equations result in two solutions for every nodal direction, where only one solution is the desired one. Using, e.g., an optimization procedure the correct geometry of the tensegrity structure can be found, although fixed nodal positions are required to remove the rigid body mode. With these DOFs removed, it is still possible not to be able to find an unique solution. Though proper initial estimates for the nodal positions in the optimization procedure can result in the correct solution, no guarantees can be given; when the structure becomes more complex, more solutions are possible. Furthermore, it is not always possible to obtain proper initial estimates. Figure 2.4 presents two possible solutions for one simple 2D tensegrity structure, defined by element lengths and the fixed nodal positions.

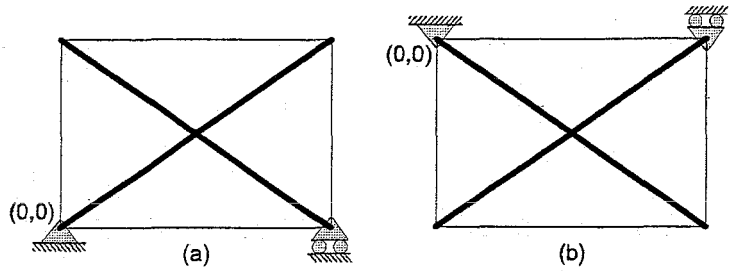

Figure 2.4: Two solutions for one tensegrity structure defined by element lengths

3D Kinematic Relations

For 3D structures the kinematic relations are derived in the same way as the 2D relations. The relations between the nodal positions and the generalized coordinates are extracted from Figure 2.1(b) and 2.2(b) and presented in Eq.(2.6) and Eq.(2.7).

$$
\begin{aligned}
q_i &= f_{qp}(p_i) \\
\begin{bmatrix} q_{x_i} \\ q_{y_i} \\ q_{z_i} \\ \theta_i \\ \varphi_i \end{bmatrix} &= \begin{bmatrix} \frac{p_{x_i}+p_{x_j}}{2} \\ \frac{p_{y_i}+p_{y_j}}{2} \\ \frac{p_{z_i}+p_{z_j}}{2} \\ \sin^{-1}\left(\frac{p_{y_j}-p_{y_i}}{a_{0_i}}\right) \\ \sin^{-1}\left(\frac{-(p_{z_j}-p_{z_i})}{L_b}\right) \end{bmatrix} \\
a_{0_i} &= \left(\left(p_{x_j}-p_{x_i}\right)^2+\left(p_{y_j}-p_{y_i}\right)^2\right)^{1/2}
\end{aligned}
\tag{2.6}
$$

$$
\begin{aligned}
p_i &= f_{pq}(q_i) \\
\begin{bmatrix} p_{x_i} \\ p_{y_i} \\ p_{z_i} \\ p_{x_j} \\ p_{y_j} \\ p_{z_j} \end{bmatrix} &= \begin{bmatrix} q_{x_i}-\frac{L_b}{2}\cos(\theta_i)\cos(\varphi_i) \\ q_{y_i}-\frac{L_b}{2}\sin(\theta_i)\cos(\varphi_i) \\ q_{z_i}+\frac{L_b}{2}\sin(\varphi_i) \\ q_{x_i}+\frac{L_b}{2}\cos(\theta_i)\cos(\varphi_i) \\ q_{y_i}+\frac{L_b}{2}\sin(\theta_i)\cos(\varphi_i) \\ q_{z_i}-\frac{L_b}{2}\sin(\varphi_i) \end{bmatrix}
\end{aligned}
\tag{2.7}
$$

The kinematic relation between nodal positions and the lengths of the elements is completely similar to the 2D kinematic relation, except that matrix C is filled with $\pm I_3$ and 0_3 and $t_i = \begin{bmatrix} t_{x_i} & t_{y_i} & t_{z_i} \end{bmatrix}^T$.

In [10], it is mentioned that Euler Angles and Tait-Briant Angles cause singularities for certain angles. In a singular configuration it is not possible to find time derivatives for the generalized coordinates. The problem of singularities can be avoided by introducing Euler

parameters (or quaternions). Instead of using three variables to describe rotations, four variables (e_0, e_1, e_2 and e_3) are applied. The idea behind Euler parameters is that every rotation can be defined as a single rotation around one vector. The rotation together with the vector can be described by the four parameters. An important property of the Euler parameters is that their length is equal to one: $e_0^2 + e_1^2 + e_2^2 + e_3^2 = 1$. For details on Euler parameters, see [10]. In this report it is sufficient to present the results:

$$
\begin{aligned}
&q_i = f_{qp}(p_i) \\
&\begin{bmatrix} q_{x_i} \\ q_{y_i} \\ q_{z_i} \\ e_{0_i} \\ e_{1_i} \\ e_{2_i} \\ e_{3_i} \end{bmatrix} = \begin{bmatrix} \frac{p_{x_i}+p_{x_j}}{2} \\ \frac{p_{y_i}+p_{y_j}}{2} \\ \frac{p_{z_i}+p_{z_j}}{2} \\ \cos\left(\frac{\theta_i}{2}\right)\cos\left(\frac{\varphi_i}{2}\right) \\ -\sin\left(\frac{\theta_i}{2}\right)\sin\left(\frac{\varphi_i}{2}\right) \\ \cos\left(\frac{\theta_i}{2}\right)\sin\left(\frac{\varphi_i}{2}\right) \\ \sin\left(\frac{\theta_i}{2}\right)\cos\left(\frac{\varphi_i}{2}\right) \end{bmatrix},
\end{aligned}
\tag{2.8}
$$

with θ_i and φ_i from Eq.(2.6).

$$
\begin{aligned}
&p_i = f_{pq}(q_i) \\
&\begin{bmatrix} p_{x_i} \\ p_{y_i} \\ p_{z_i} \\ p_{x_j} \\ p_{y_j} \\ p_{z_j} \end{bmatrix} = \begin{bmatrix} q_{x_i} - \frac{L_b}{2}\left(e_{0_i}^2 + e_{1_i}^2 - e_{2_i}^2 - e_{3_i}^2\right) \\ q_{y_i} - L_b\left(e_{1_i}e_{2_i} + e_{0_i}e_{3_i}\right) \\ q_{z_i} - L_b\left(e_{1_i}e_{3_i} - e_{0_i}e_{2_i}\right) \\ q_{x_i} + \frac{L_b}{2}\left(e_{0_i}^2 + e_{1_i}^2 - e_{2_i}^2 - e_{3_i}^2\right) \\ q_{y_i} + L_b\left(e_{1_i}e_{2_i} + e_{0_i}e_{3_i}\right) \\ q_{z_i} + L_b\left(e_{1_i}e_{3_i} - e_{0_i}e_{2_i}\right) \end{bmatrix}
\end{aligned}
\tag{2.9}
$$

The remainder of the report uses generalized coordinates defined by Euler parameters.

2.3 Dynamics, using Euler parameters

The derivation of the dynamics is done using Newton-Euler equations. The generalized coordinates are used to describe these equations of motion. The basis for derivation of the dynamics has already been presented in [9]. In this Section however, the dynamics will be expressed using Euler parameters instead of Tait-Bryant Angles.
In Subsection 2.3.1 the standard Newton-Euler equations are derived. In Subsection 2.3.2 the influence of restrictions, i.e., fixed nodal positions, on the dynamic equations is presented. This Section ends with the presentation of the final dynamic equations in Subsection 2.3.3.

2.3.1 Basic Newton-Euler dynamics

For the description of the dynamics of an arbitrary Class 1 tensegrity structure Newton-Euler equations are used. The translational acceleration is given by the Newton equation, Eq.(2.10), while angular accelerations are derived using Euler equations, Eq.(2.11). The translational acceleration of the center of mass of bar i is given by $\ddot{r}_i = [\ddot{q}_{x_i}\ \ddot{q}_{y_i}\ \ddot{q}_{z_i}]^T$, the angular velocity is presented by ω_i.
During the derivations of the equations, two frames or coordinate basis are used. The first frame $\underline{\vec{e}}^{\,0}$ is the reference frame. The second frame $\underline{\vec{e}}^{\,1}$ is a local frame, with the local x-axis in the length direction of a bar. The centers of mass r are defined in $\underline{\vec{e}}^{\,0}$ and the angular velocities ω in $\underline{\vec{e}}^{\,1}$.

$$
\begin{aligned}
F_{b_i} &= m_i\ddot{r}_i && (2.10)\\
M_{b_i} &= \mathbb{J}\dot{\omega}_i + \omega_i \otimes (\mathbb{J}_i \cdot \omega_i) && (2.11)\\
\text{and } F_b &= \begin{bmatrix} F_{b_1}^T & F_{b_2}^T & \cdots & F_{b_{n_b}}^T \end{bmatrix}^T \text{ and } M_b = \begin{bmatrix} M_{b_1}^T & M_{b_2}^T & \cdots & M_{b_{n_b}}^T \end{bmatrix}^T
\end{aligned}
$$

In Eq.(2.10) F_{b_i} is the resulting force that works on the bar and m_i is the mass of the bar. In Eq.(2.11) M_{b_i} presents the resulting momentum working on the center of mass of the bar and $\mathbb{J}_i$ is the tensor containing the different inertias of the bar.
The resulting force F_{b_i} and momentum M_{b_i} can be calculated using Eq.(2.12).

$$
\begin{aligned}
F_{b_i} &= F_{n1_i} + F_{n2_i} + m_i G, \qquad M_{b_i} = c_{1i} \otimes F_{n1_i} + c_{2i} \otimes F_{n2_i}, && (2.12)\\
\text{with } c_{1i} &= \begin{bmatrix} -0.5L_{b_i} & 0 & 0 \end{bmatrix} \underline{\vec{e}}^{\,1} \text{ and } c_{2i} = \begin{bmatrix} 0.5L_{b_i} & 0 & 0 \end{bmatrix} \underline{\vec{e}}^{\,1} && (2.13)
\end{aligned}
$$

The vectors c_{1i} and c_{2i} define the distance from the center of mass to the ends of the bar. Note that they are expressed in the local frame $\underline{\vec{e}}^{\,1}$. The forces F_{n1_i} and F_{n2_i} are the resulting forces working on the two ends of the bar, expressed in $\underline{\vec{e}}^{\,0}$. The length of the bar is presented by L_b and G presents the gravitational vector in $\underline{\vec{e}}^{\,0}$. The transformation of the nodal forces from $\underline{\vec{e}}^{\,0}$ to $\underline{\vec{e}}^{\,1}$ will be discussed later on in this section.
The steps taken to determine the nodal force F_n are presented in Eq.(2.14) and Eq.(2.15). The one-sidedness of the linear spring is expressed as $\max(0, L_t - L_{t_0})$, with L_{t_0} the rest length of the tendon. When the elongation of the tendon is positive this results in a tensile force. When the elongation is negative, no force is present. In case damping is present in the tendon d_{damp} should be given a positive value.

$$
\begin{aligned}
F_n &= -C_t^T F_t + w, \text{ with } F_t = \begin{bmatrix} F_{t_1}^T & F_{t_2}^T & \cdots & F_{t_{n_t}}^T \end{bmatrix}^T && (2.14)\\
F_{t_i} &= max\left(0,\ L_{t_i} - L_{t_{0_i}}\right) \left(\frac{E_i A_{t_i}}{L_{t_{0_i}}} + \frac{d_{damp}(\dot{L}_{t_i} - \dot{L}_{t_{0_i}})}{L_{t_i} - L_{t_{0_i}}} \right) \frac{\pm t_i}{L_{t_i}} && (2.15)
\end{aligned}
$$

In Eq.(2.15), $\pm$ describes the direction of the force vector with respect to the direction of t, since they are aligned [4]. When the force vector and the element vector have the same

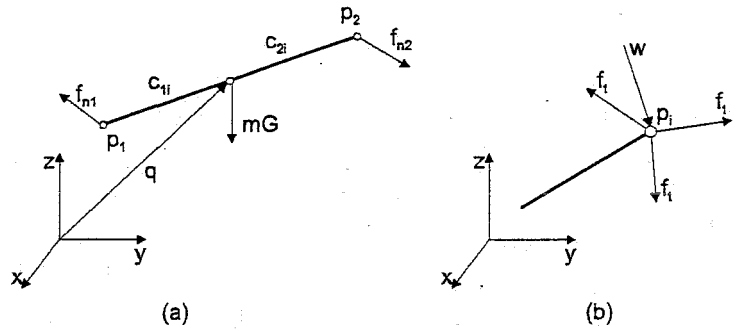

Figure 2.5: a) Resulting forces working on a bar, b) Tendon and external forces working on a node

direction $\pm$ becomes $+$. For opposite directions, $\pm$ must be $-$. In Eq.(2.14) the $\pm$ is not needed anymore, since it is already present in C_t.
The external forces, e.g., an extra weight on a node or a random disturbance like wind, are gathered in the vector w. The Young's modulus is presented by E and the cross sectional area of the tendon by A_t. In Figure 2.5 the forces working on a bar are illustrated.

For the momentum equations, expressions for the angular velocity ω and angular acceleration $\dot{\omega}$ have to be derived. The rotation tensor R, needed for ω, is presented in Eq.(2.16).

$$R^T = \begin{bmatrix} e_0^2+e_1^2-e_2^2-e_3^2 & 2(e_1e_2+e_0e_3) & 2(e_1e_3-e_0e_2) \\ 2(e_1e_2-e_0e_3) & e_0^2-e_1^2+e_2^2-e_3^2 & 2(e_2e_3+e_0e_1) \\ 2(e_1e_3+e_0e_2) & 2(e_2e_3-e_0e_1) & e_0^2-e_1^2-e_2^2+e_3^2 \end{bmatrix} \tag{2.16}$$

A standard method for finding the angular velocity is presented in Eq.(2.17).

$$^{10}\omega^1 = R^T\dot{R} = \begin{bmatrix} 0 & -^{10}\omega_3^1 & ^{10}\omega_2^1 \\ ^{10}\omega_3^1 & 0 & -^{10}\omega_1^1 \\ -^{10}\omega_2^1 & ^{10}\omega_1^1 & 0 \end{bmatrix} \tag{2.17}$$

$^{10}\omega$ denotes that the rotation is in the local frame $\underline{\vec{e}}^{\,1}$ with respect to the global frame $\underline{\vec{e}}^{\,0}$. The notation ω^1 refers to the fact that the angular velocity is expressed in the local frame. The subscripts correspond to the three axis of the local frame.
Solving Eq.(2.17) results in the angular velocity Eq.(2.18). Differentiating $\vec{\omega}$ results in the angular acceleration $\dot{\omega}$, Eq.(2.19). The relation between the two frames is $\underline{\vec{e}}^{\,1} = R^T\underline{\vec{e}}^{\,0}$.

$$\omega^1 = \begin{bmatrix}\omega_1\\ \omega_2\\ \omega_3\\ 0\end{bmatrix} = \begin{bmatrix}-2e_1 & 2e_0 & 2e_3 & -2e_2\\ -2e_2 & -2e_3 & 2e_0 & 2e_1\\ -2e_3 & 2e_2 & -2e_1 & 2e_0\\ e_0 & e_1 & e_2 & e_3\end{bmatrix}\begin{bmatrix}\dot{e}_0\\ \dot{e}_1\\ \dot{e}_2\\ \dot{e}_3\end{bmatrix} = \begin{bmatrix}W_1\\ W_2\\ W_3\\ W_4\end{bmatrix}\omega^* \qquad (2.18)$$

$$\dot{\omega}^1 = \begin{bmatrix}\dot{\omega}_1\\ \dot{\omega}_2\\ \dot{\omega}_3\\ 0\end{bmatrix} = \begin{bmatrix}W_1\\ W_2\\ W_3\\ W_4\end{bmatrix}\dot{\omega}^* \qquad (2.19)$$

$$\text{with } \omega^* = \begin{bmatrix}\dot{e}_0 & \dot{e}_1 & \dot{e}_2 & \dot{e}_3\end{bmatrix}^T \text{ and } \dot{\omega}^* = \begin{bmatrix}\ddot{e}_0 & \ddot{e}_1 & \ddot{e}_2 & \ddot{e}_3\end{bmatrix}^T$$

The fourth equations in Eq.(2.18) and Eq.(2.19) are obtained by taking the time derivatives of $e_0^2 + e_1^2 + e_2^2 + e_3^2 = 1$. In [11], using quaternion algebra, similar equations for the angular velocity and acceleration have been derived.
In [12] and [13] the dependency in the Euler parameters is seen as a kinematic constraint and integrated in the dynamics by introducing Lagrange multipliers. In this report the dependency is removed by defining the *time* derivatives of *one* Euler parameter as function of the others. This way, the actual constraint is removed from the dynamics and indirect relations (time-derivatives of the constraint) are introduced. This makes it possible to avoid the use of Lagrange multipliers. The real constraint can be recovered by integrating the time-derivatives. However, simulation errors in the time-derivatives, e.g., rounding errors, will be integrated as well, resulting in possible cumulation of the error in the actual constraint in time.
This report will only deal with simulation times smaller than or equal to 1.5 seconds. It is assumed that cumulation of errors will remain small enough, so that errors in the actual constraint in the Euler parameters are not noticeable. In the example in Chapter 5 the assumption is checked for correctness. If not, Lagrange multipliers can be introduced, or stabilizing projections can be applied to correct for the simulation errors.
In Eq.(2.20) $W_4\omega^* = 0$, related to the first time-derivative of the dependency in the Euler parameters, is rewritten for all four Euler parameters. All four options should be present in the dynamic model for the situation that the denominator of the first chosen equation equals zero. The equation for the second time derivative is properly integrated in the momentum equation (Eq.(2.21), fourth equation).

$$\begin{aligned}
\dot{e}_0 &= -\frac{e_1\dot{e}_1 + e_2\dot{e}_2 + e_3\dot{e}_3}{e_0}\\
\dot{e}_1 &= -\frac{e_0\dot{e}_0 + e_2\dot{e}_2 + e_3\dot{e}_3}{e_1}\\
\dot{e}_2 &= -\frac{e_0\dot{e}_0 + e_1\dot{e}_1 + e_3\dot{e}_3}{e_2}\\
\dot{e}_3 &= -\frac{e_0\dot{e}_0 + e_1\dot{e}_1 + e_2\dot{e}_2}{e_3}
\end{aligned} \qquad (2.20)$$

Solving the righthand side of Eq.(2.11) in the local frame $\underline{\vec{e}}^{\,1}$ for bar i, using $\mathbb{J} = diag\begin{bmatrix} J_x & J & J \end{bmatrix}$, results in Eq.(2.21). The inertia J_x represents the inertia related to rotations in the axial direction of the bar. The inertia J corresponds to rotations in the $\underline{\vec{e}}_2^{\,1}$ and $\underline{\vec{e}}_3^{\,1}$ direction and is identical for both directions.

$$\begin{aligned} \mathbb{J}\dot{\omega}_i + \omega_i \otimes (\mathbb{J} \cdot \omega_i) &= \begin{bmatrix} J_x W_1 \\ J\ W_2 \\ J\ W_3 \\ W_4 \end{bmatrix} \dot{\omega}_i^* + \begin{bmatrix} 0 \\ (J_x - J) W_3 \omega_i^* W_1 \omega_i^* \\ (J - J_x) W_1 \omega_i^* W_2 \omega_i^* \\ {\omega_i^*}^T \omega_i^* \end{bmatrix} \qquad (2.21) \\ \mathbb{J}\dot{\omega}_i + \omega_i \otimes (\mathbb{J} \cdot \omega_i) &= M_1 \dot{\omega}_i^* + M_2 \qquad (2.22) \end{aligned}$$

To complete the rewriting of the basic dynamic equations, the lefthand side of Eq.(2.11) must be worked out. First it must be noted that the righthand side is expressed in the local $\underline{\vec{e}}^{\,1}$ frame. Therefor the lefthand side should also be expressed in this frame. The nodal forces F_n are originally expressed in $\underline{\vec{e}}^{\,0}$ and must thus be rewritten to $\underline{\vec{e}}^{\,1}$: $F_{n_i}^1 = R^T F_{n_i}$. To simplify some notations, the first values (scalars) in the vectors c_{1i} and c_{2i} for a bar are given by:

$$c_i^1 = c_{1i}(1) \quad \text{and} \quad c_i^2 = c_{2i}(1) \qquad (2.23)$$

The cross products in the equation result in:

$$\begin{aligned} M_{b_i} &= c_{1i} \otimes F_{n1_i} + c_{2i} \otimes F_{n2_i} \\ M_{b_i} &= c_i^1 C_{cross} F_{n1_i}^1 + c_i^2 C_{cross} F_{n2_i}^1 \\ M_{b_i} &= c_i^1 C_{cross} R^T F_{n1_i} + c_i^2 C_{cross} R^T F_{n2_i} \qquad (2.24) \\ \text{with } C_{cross} &= \begin{bmatrix} 0 & 0 & 0 \\ 0 & 0 & -1 \\ 0 & 1 & 0 \end{bmatrix} \end{aligned}$$

Gathering all the momenta M_{b_i} results in Eq.(2.25).

$$M_b = C_a F_n \qquad (2.25)$$

The matrix C_a is obtained by replacing the elements $-I_3$ and I_3 in C_b by $c_i^1 C_{cross} R^T$ and $c_i^2 C_{cross} R^T$ respectively [9]. This is graphically illustrated by Figure 2.6.

$$\begin{bmatrix} -I_3 & 0_3 & 0_3 & I_3 \\ 0_3 & -I_3 & I_3 & 0_3 \end{bmatrix} \longrightarrow \begin{bmatrix} c^1{}_1 C_{cross} R_1^T & 0_3 & 0_3 & c^2{}_1 C_{cross} R_1^T \\ 0_3 & c^1{}_2 C_{cross} R_2^T & c^2{}_2 C_{cross} R_2^T & 0_3 \end{bmatrix}$$

Figure 2.6: Example of how C_a is obtained from C_b

2.3.2 Restrictions

Every tensegrity structure has to be fixed to a reference frame in order to eliminate the rigid body mode, e.g., by joints. A joint fixes a node in one or more directions and has influence on the dynamics of the tensegrity structure. In this Subsection, changes in the dynamics inflicted by the joints are derived. As with the dependency in the Euler parameters, not the actual constraints are integrated in the dynamics, but their time-derivatives. This is again done to avoid the use of Lagrange multipliers.
The position of a node with respect to the center of mass of the bar is given by Eq.(2.26). In this Subsection, node 1 of the bar is chosen to be fixed. To fix node 2, change c_i^1 to c_i^2.

$$p_j = r_i + c_i^1 \begin{bmatrix} e_0^2 + e_1^2 - e_2^2 - e_3^2 \\ 2(e_1e_2 + e_0e_3) \\ 2(e_1e_3 - e_0e_2) \end{bmatrix} \tag{2.26}$$

Since the node is fixed, the velocity and the acceleration of the node is zero. The expressions for the velocity and acceleration of the center of mass are presented in Eq.(2.28) and Eq.(2.31) respectively.

$$\dot{p}_j = 0 \tag{2.27}$$

$$\dot{p}_j = \dot{r}_i + 2c_i^1 \begin{bmatrix} e_0 & e_1 & -e_2 & -e_3 \\ e_3 & e_2 & e_1 & e_0 \\ -e_2 & e_3 & -e_0 & e_1 \end{bmatrix} \omega_i^* \tag{2.28}$$

$$\dot{r}_i = -2c_i^1 E_p \omega_i^* \tag{2.29}$$

$$\ddot{p}_j = 0 \tag{2.30}$$

$$\begin{aligned} \ddot{p}_j = \ddot{r}_i &+ 2c_i^1 \begin{bmatrix} e_0 & e_1 & -e_2 & -e_3 \\ e_3 & e_2 & e_1 & e_0 \\ -e_2 & e_3 & -e_0 & e_1 \end{bmatrix} \dot{\omega}_i^* \\ &+ 2c_i^1 \begin{bmatrix} \dot{e}_0 & \dot{e}_1 & -\dot{e}_2 & -\dot{e}_3 \\ \dot{e}_3 & \dot{e}_2 & \dot{e}_1 & \dot{e}_0 \\ -\dot{e}_2 & \dot{e}_3 & -\dot{e}_0 & \dot{e}_1 \end{bmatrix} \omega_i^* \end{aligned} \tag{2.31}$$

$$\ddot{r}_i = -2c_i^1 E_p \dot{\omega}_i^* - 2c_i^1 \dot{E}_p \omega_i^* = -R_{r1}\dot{\omega}_i^* - R_{r2} \tag{2.32}$$

Restrictions introduce unknown reaction forces in the fixed node. Eq.(2.33) presents the equation for these unknown reaction forces. It is clear that this equation is nothing more than rewriting the first equation of Eq.(2.12).

$$F_{restrict} = m_i\ddot{r}_i - F_{n2_i} - m_iG \tag{2.33}$$

Using Eq.(2.33) to replace F_{n1_i} in the second equation of Eq.(2.12) a new expression for the momentum can be derived. This derivation is given in Eq.(2.34-2.38). As a consequence of this replacement, the momentum equation is shifted from the center of mass to node 1.

This results in the introduction of the mass in the momentum equation. Assuming for now that all directions are fixed, this equations are only a function of the Euler parameters.

$$
\begin{aligned}
M_{b_i} &= c_i^1 C_{cross} R^T F_{restrict} + c_i^2 C_{cross} R^T F_{n2_i} && (2.34)\\
&= c_i^1 C_{cross} R^T (m_i \ddot{r}_i - F_{n2_i} - m_i G) + c_i^2 C_{cross} R^T F_{n2_i} && (2.35)\\
&= c_i^1 C_{cross} R^T m_i \ddot{r}_i + L_{b_i} C_{cross} R^T F_{n2_i} - c_i^1 C_{cross} R^T m_i G && (2.36)\\
&= c_i^1 C_{cross} R^T m_i (-R_{r1} \dot{\omega}_i^* - R_{r2}) + L_{b_i} C_{cross} R^T F_{n2_i} \\
&\quad - c_i^1 C_{cross} R^T m_i G && (2.37)\\
&= -M R_1 \dot{\omega}_i^* - M R_2 + L_{b_i} C_{cross} R^T F_{n2_i} - M R_3 && (2.38)
\end{aligned}
$$

The matrix C_a has to be altered, since now only F_{n2_i} is present in the momentum equation. The part $c_i^1 C_{cross} R^T$ is set to 0_3 and $c_i^2 C_{cross} R^T$ to $L_{b_i} C_{cross} R^T$.
When all directions of node 1 are fixed, integrating Eq.(2.38) into the dynamic model will successfully handle the restrictions in the system. How to do this, will be presented in the next Subsection.
However, it can also be possible that node 1 is partially restricted. The alternations that have to be made are:

- Eq.(2.28) and Eq.(2.31) are only valid in the directions in which the node is restricted. If, e.g., node 1 is fixed in the global x and z direction, the second, y direction, of the three equations has to be set to zero. This is done by setting the corresponding value in R_{r2} and row in R_{r1} to zero.
- In Eq.(2.33), the forces related to the directions that are not restricted, should be set to zero (these directions simply use the first equation in Eq.(2.12)). Partly this has already been accomplished by adjusting R_1 and R_2. The components of the gravity vector G related to the free directions, have to be set to zero as well.
- In the C_a, which includes the restrictions, some extra changes have to be made. The columns in C_a, corresponding to the free directions, must have the old values of the original C_a, since the basic dynamics must be applied here.

If node 2 is fixed, C_a must be altered from $c_i^1 C_{cross} R^T$ and $c_i^2 C_{cross} R^T$ to $-L_b C_{cross} R^T$ and 0_3 respectively.

As an example of how to obtain the correct C_a, in Figure 2.7 a schematic presentation of the changes in C_a is given. Here node 1 of bar 2 is 1) not restricted, 2) completely fixed, 3) y direction of the restricted node is free.

2.3.3 Final equations of motion

To conclude the dynamics of a tensegrity structure, the final equations of motion are presented in this Subsection. The equations related to the translations are presented in

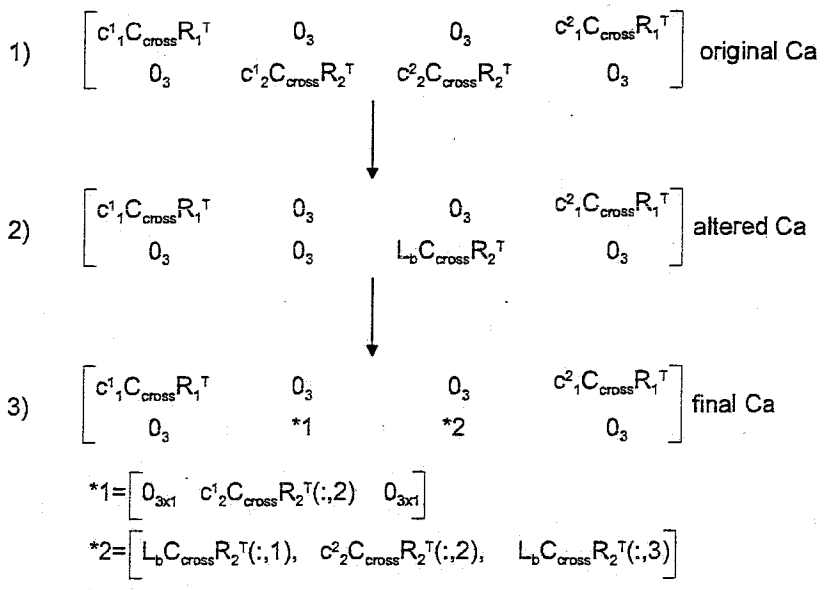

Figure 2.7: Changes in C_a: First, node 1 of bar 2 has no restrictions. Second, node 1 of bar 2 is completely fixed, Third, y direction of the restricted node 1 of bar 2 is free

Eq.(2.39), with r the centers of mass of all bars. The mass matrices M_m and M_{m2} are presented in Eq.(2.40).

$$M_m\ddot{r} = F_{n1} + F_{n2} + M_{m2}G = |C_b|F_n + M_{m2}G \tag{2.39}$$

$$M_m = \begin{bmatrix} m_1 I_3 & \cdots & 0_3 \\ \vdots & \ddots & \vdots \\ 0_3 & \cdots & m_{n_b} I_3 \end{bmatrix}, \quad M_{m2} = \begin{bmatrix} m_1 I_3 \\ \vdots \\ m_{n_b} I_3 \end{bmatrix} \tag{2.40}$$

The rows and columns in the mass matrix M_m and C_b related to restricted directions, should be removed. The same goes for the rows in M_{m2}. This way, the equations of motion related to the restrictions are removed from the final equations of motion.
For the angular accelerations, the restrictions are build in into the different vectors and matrices. Remember from Eq.(2.21) that there are four equations per bar, while the momentum equations, i.e., Eq.(2.25) and Eq.(2.38), only result in three. The fourth equation is related to the second time-derivative of the dependency in the Euler parameters and equals zero. To include the extra equation in (2.25) and (2.38) an extra zero must be added to MR_2, MR_3 and $C_{a_i}F_n$, and a row with zeros in MR_1. This results in $MR_2^* = [MR_2; 0]$, $MR_3^* = [MR_3; 0]$, $M_b^* = [C_{a_i}F_n; 0]$ and $MR_1^* = [MR_1; \mathbf{0}]$. The notation C_{a_i} refers to the rows in C_a corresponding to bar i.
Using the short notations, the equations for the angular accelerations for bar i are given in Eq.(2.41).

$$
\begin{aligned}
(M_1 + MR_1^*)\,\dot{\omega}_i^* &= (-M_2 - MR_2^* - MR_3^* + M_b^*) \\
\dot{\omega}_i^* &= (M_1 + MR_1^*) \setminus (-M_2 - MR_2^* - MR_3^* + M_b^*)
\end{aligned} \tag{2.41}
$$

2.4 Statics

It is important that a tensegrity structure keeps its integrity. A sufficient condition to guarantee this, is that no tendons are allowed to go slack. When a tendon does go slack it can be compared with removing a spring from the system, which can result in an abrupt change in stiffness of the system. Keeping all tendons under tension thus guarantees the smoothness of the stiffness of the tensegrity structure during the shape trajectory, which is desired.
A way to check slackness of tendons is to determine the forces in the tendons. If the forces in the tendons are greater than zero, tensile forces are present in the tendons and integrity is guaranteed. However, tensegrity structures are redundant systems, i.e., are over-determined. When constitutive equations are omitted, only force ratios can be determined. This is caused by the fact that there are more tendon forces than force equations. If there are external forces working on the system, e.g., extra masses, the corresponding forces can be included in the algorithm in the vector w.
Depending on the presence or absence of gravity in the system, two optimization approaches for finding the forces are presented. In Subsection 2.4.1 an optimization algorithm is presented when no gravity works on the system. Subsection 2.4.2 handles the case where gravity is present.

2.4.1 Statics in absence of gravity

Without gravity, the optimization algorithm can be derived from Figure 2.5(b). Although the bar force is not present in Figure 2.5(b) it will be used for the optimization. The idea behind this approach is that the sum of all the forces working on a node should equal zero; when there are no resulting forces working on the nodes, there will be no translational or rotational movements. The result is presented in Eq.(2.42), with the * indicating the magnitude of a force vector. In Eq.(2.42) n denotes the total number of tendons attached to node i, with node i attached to bar k. Since this study only deals with Class 1 tensegrity structures, only one bar force is present in the equation.

$$
\begin{aligned}
\sum_{j=1}^{n} \pm F_{t_{i,j}} \pm F_{b_k} + w_i &= 0, \quad \text{with } F_{t_{i,j}} = \frac{t_j}{L_{t_j}} F^*_{t_{i,j}} \\
\sum_{j=1}^{n} \frac{\pm t_j}{L_{t_j}} F^*_{t_{i,j}} + \frac{\pm t_{n_t+k}}{L_{b_k}} F^*_{b_k} &= -\begin{bmatrix} w_{x_i} \\ w_{y_i} \\ w_{z_i} \end{bmatrix}
\end{aligned} \tag{2.42}
$$

In Eq.(2.42), $\pm$ again describes the direction of the force vector with respect to the direction of t. When all node equations are collected Eq.(2.43) is found. The aspect of $\pm$ is of no

importance anymore, since it is already present in the topology matrix C. In vector F^* all $n_t + n_b$ magnitudes of the forces are gathered. The vector w represents the external forces on all nodes and has length $D \cdot 2n_b$, since there are $D \cdot 2n_b$ nodal directions in the structure. D represents the number of dimensions of the structure and is 2 for 2D structures and 3 for 3D.

$$A_{eq}F^* = w \tag{2.43}$$

$$\text{with } A_{eq} = C^T \begin{bmatrix} \frac{t_1}{L_{t_1}} & 0_{D\times 1} & \cdots & 0_{D\times 1} \\ 0_{D\times 1} & \frac{t_2}{L_{t_2}} & \cdots & 0_{D\times 1} \\ \vdots & \vdots & \ddots & \vdots \\ 0_{D\times 1} & 0_{D\times 1} & \cdots & \frac{t_{n_t+n_b}}{L_{b_{n_b}}} \end{bmatrix}, \quad F^* = \begin{bmatrix} F_t^* \\ F_b^* \end{bmatrix} \text{ and } b_{eq} = w = \begin{bmatrix} w_1 \\ w_2 \\ \vdots \\ w_{2n_b} \end{bmatrix}$$

Eq.(2.43) represents the equality constraint in the optimization algorithm. The other constraint is that $F_t^* \geq \alpha$ with $\alpha > 0$, due to the fact that the tendons are not allowed to go slack.

For linear optimization the objective function, i.e., the function to be minimized, can be the sum of the forces $(\sum F_t^* - \sum F_b^*)$. This objective assumes that F_b^* is smaller than or equal to zero. For quadratic optimization the objective function can be of the form $F^{*^T}F^*$. Solving the optimization results in force ratios. With α set to the minimum allowed tensile force, the actual forces in all elements can be found.

The quadratic optimization is preferred over the linear optimization. With changes in configuration quadratic optimization will result in a 'smoother' force transition in the elements than the linear optimization. Furthermore, the assumption that $F_b^* \leq 0$ does not have to be true. The optimization algorithm can be summarized as:

$$\min \; F^{*^T}F^*, \text{ sub } A_{eq}F^* = b_{eq} \tag{2.44}$$

$$F_t^* \geq \alpha > 0 \tag{2.45}$$

2.4.2 Statics in presence of gravity

The basis for finding the element forces in systems subject to gravity is presented in Figure 2.5 a). The approach is based on the dynamic equations in which all time derivatives have been set to zero. By doing this, a static situation is created. The following equations are derived from Eq.(2.39) (related to the force equations) and Eq.(2.25) (related to the momentum equations):

$$0 = F_{n1} + F_{n2} + M_{m2}G = |C_b|F_n + M_{m2}G \tag{2.46}$$

$$0 = C_a F_n \tag{2.47}$$

In the force equations restrictions must me accounted for. In Eq.(2.48) to Eq.(2.51) this can be done by removing the rows of $|C_b|$ and M_{m2} related to restricted directions. Remember from Eq.(2.14) that $F_n = -C_t^T F_t + w$.

$$
\begin{aligned}
-|C_b|F_n &= M_{m2}G && (2.48)\\
-|C_b|(-C_t^T F_t + w) &= M_{m2}G && (2.49)\\
|C_b|C_t^T F_t &= |C_b|w + M_{m2}G && (2.50)\\
|C_b|C_t^T t_{mat} F_t^* &= |C_b|w + M_{m2}G && (2.51)
\end{aligned}
$$

$$
\text{with } t_{mat} = \begin{bmatrix} \frac{t_1}{L_{t_1}} & 0_{D\times 1} & \cdots & 0_{D\times 1} \\ 0_{D\times 1} & \frac{t_2}{L_{t_2}} & \cdots & 0_{D\times 1} \\ \vdots & \vdots & \ddots & \vdots \\ 0_{D\times 1} & 0_{D\times 1} & \cdots & \frac{t_{n_t}}{L_{t_{n_t}}} \end{bmatrix}
$$

$$
A_{eq_F} F_t^* = b_{eq_F} \qquad (2.52)
$$

For bars that have no restrictions the momentum equations are presented in Eq.(2.55). In the equations, C_a corresponds to the original C_a of Eq.(2.25).

$$
\begin{aligned}
0 &= C_a F_n = C_a(-C_t^T F_t + w) && (2.53)\\
C_a C_t^T F_t &= C_a w && (2.54)\\
C_a C_t^T t_{mat} F_t^* &= C_a w && (2.55)
\end{aligned}
$$

The momentum equations, including the restricted bars, are presented in Eq.(2.56). The matrix C_a includes the changes introduced by the restrictions, as has already been illustrated by Figure 2.7, 3). The components of the gravity vector $F_G = [G_1^T, G_2^T, \cdots, G_{n_b}^T]^T$ that do not relate to restricted directions must be set to zero. The factor of $0.5F_G$ corresponds to the fact that the center of mass is positioned halfway the bars.

$$
\begin{aligned}
C_a C_t^T t_{mat} F_t^* &= C_a(w + 0.5F_G) && (2.56)\\
A_{eq_{Mb}} F_t^* &= b_{eq_{Mb}} && (2.57)
\end{aligned}
$$

The optimization algorithm is defined by:

$$
\min F_t^{*T} F_t^*, \text{ sub } \begin{bmatrix} A_{eq_F} \\ A_{eq_{Mb}} \end{bmatrix} F_t^* = \begin{bmatrix} b_{eq_F} \\ b_{eq_{Mb}} \end{bmatrix} \qquad (2.58)
$$

$$
F_t^* > \alpha > 0 \qquad (2.59)
$$

As can be seen the optimization algorithm only determines the tendon forces. A bar force can be determined using Eq.(2.60) and Eq.(2.61), depending on which node of the bar is restricted. Eq.(2.60) is related to bars restricted at the first node and Eq.(2.61) to bars restricted at the second node of a bar. When a bar is not fixed, both equations can be used. The reason for two equations is, that reaction forces in a restricted node are unknown and thus cannot be used to determine bar forces.

$$F_{b_i} = \frac{t_{b_i}^T}{L_{b_i}} F_{n_{2_i}} \tag{2.60}$$

$$F_{b_i} = -\frac{t_{b_i}^T}{L_{b_i}} F_{n_{1_i}} \tag{2.61}$$

Chapter 3

Reference trajectory generator

This Chapter presents an optimization method for finding a shape trajectory for shape changes of an arbitrary Class 1 tensegrity structure. In [6] the deployment for a Class 1 tensegrity structure has been investigated. However the shape of the studied tensegrity structure is defined by one parameter only and the deployment is related to variations of this one parameter. This type of shape change is not very useful for an arbitrary Class 1 tensegrity structure or trajectory.
The optimization method introduced in this Chapter has a number of similarities to [5] and [14]. In [5], not the optimization for shape change is investigated, but the optimization of the mass to stiffness of a tensegrity structure. In [14] the existence of an arbitrary truss structure has been studied. Both papers define an optimization problem, subject to several constraints. A number of constraints related to forces and element lengths presented in these papers are also applicable to the optimization method presented in this Chapter.

Throughout the shape change of a tensegrity structure, there are several constraints that have to be satisfied. These constraints consist of singularity avoidance, collision detection, and force signature and magnitude constraints. Sections 3.1, 3.2, and 3.3, respectively, will discuss these items.
Due to the extensiveness and complexity of the checks, for relatively fast shape changes, they cannot be performed on-line. Therefor an off-line method is introduced for finding a shape trajectory that satisfies all the constraints. When the actual shape change is performed, a feedback controller will only have to follow the reference trajectory, and suppress external disturbances and effects of modelling errors. The feedback controller does not have to deal with constraint satisfaction. The design of this reference trajectory is discussed in Section 3.4.

3.1 Singularity avoidance

A system is singular when its configuration results in loss of a degree of freedom (DOF) in movement. Figure 3.1 presents two singular configurations of a three link planar robot. The arrow represent the lost DOF, i.e., the direction in which the output, in this case the

tip-position of the planar robot, cannot be moved easily or move at all.

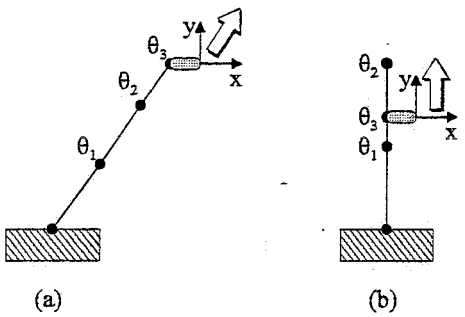

Figure 3.1: Singular configurations with a three link planar robot

To successfully control a robot, singularities have to be avoided. In order to counteract for singular configurations, they can be an integral part of the control strategy [15], [16]. Avoiding singularities not only results in better control of a system, it also decreases the chance of failure of a system due to, e.g., locked joints [17], [18] and [19].

3.1.1 Singularity in regular systems

The tip position of the three link planar robot presented in Figure 3.1 is given by the forward kinematic equation Eq.(3.1), where X is the tip position of the robot and Θ contains the joint angles. In order to perform a point-to-point movement of the tip, the joint angles have to be formulated as a function of the desired tip position. The corresponding inverse kinematic equation is given by Eq.(3.2). For redundant systems the pseudo-inverse f^+ of f can be taken, with $f^+ = f^T(ff^T)^{-1}$ for under-constrained (fat) systems and $f^+ = (f^Tf)^{-1}f^T$ for over-constrained (tall) systems, assuming full rank of f.

$$X = \begin{bmatrix} x \\ y \end{bmatrix} = f(\Theta) \tag{3.1}$$

$$\Theta = f^{-1}(X) \tag{3.2}$$

Singularities can be detected by investigating the time derivative of the inverse kinematic equation, presented by Eq.(3.3).

$$\dot{\Theta} = \frac{d}{dt} f^{-1}(X) = \frac{\partial f^{-1}(X)}{\partial X} \dot{X} = J(X)\dot{X} \tag{3.3}$$

In Eq.(3.3) $J(X)$ is the Jacobian matrix of $f^{-1}(X)$. When $J(X)$ looses rank, it looses a DOF and singularity occurs.
In [15] several performance indices for the manipulability of a robot are presented. The indices correspond to how close a system is to a singular configuration. Most commonly used indices are related to the singular values, σ_i, of $J(X)$.

One index for manipulability is the Minimum Singular Value and is related to the minimum singular value of the Jacobian. The smaller σ_{min}, the more difficult it will be to manipulate the corresponding DOF or linear combinations of DOFs. When σ_{min} approaches zero, $J(X)$ looses rank and singularity occurs.
Another index for manipulability is the Condition Number. It is defined as $\sigma_{max}/\sigma_{min}$, and represents the maximum difference in manipulability of the DOF. The optimal value of the Condition Number is 1, which means that all DOF are equally manipulable.

3.1.2 Singularity in tensegrity structures

Manipulability in tensegrity structures is related to the possibility to move both nodes of a bar in 2 or 3 (dependent on the dimension of the structure) independent directions. Hereby it is assumed that bars are stiff and cannot actively influence the position of the nodes. With this assumption bars can be excluded from the manipulability analysis.
It is not necessary for tendons to actually be connected to a bar, to influence its position. A disadvantage of influencing the position of a bar with tendons that are indirectly connected to the bar is, that a larger part of the tensegrity structure has to be moved in order to accomplish the displacement. This can result in a new configuration of the structure, which can be undesirable. Therefor manipulability of a tensegrity structure in this research is defined as the possibility to alter the positions of the nodes of a bar by influencing the length of the tendons *connected to that bar.*
A tendon can only actively influence the position of a node by shortening its length. Possibly other tendon lengths will have to increase in order to reposition the node to a desired position. However, using the definition of manipulability of a tensegrity structure at least one tendon, connected to the bar to which the node is attached, should be shortened. This can be illustrated by the example showing the opposite: all tendon lengths attached to a bar are increased more than the elongation caused by the tension in the tendons. In this case, some tendons will go slack and the bar will be able to (partially) move freely in space. This is undesired since the integrity of the structure cannot be assured anymore.
Figure 3.2a) presents a normal tensegrity structure: the nodes of the bars can be moved in all directions by shortening at least one tendon attached to the corresponding bar. Figure 3.2b) presents a tensegrity structure that is close to singularity: it is almost not possible to move the lower left node in the direction of the arrow. Figure 3.2c) presents the final singular configuration of Figure 3.2b).

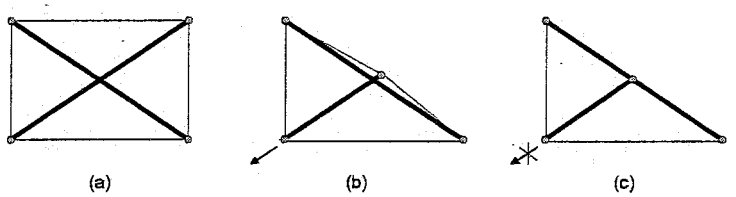

Figure 3.2: a) A normal 2D tensegrity structure, b) a tensegrity structure close to a singular configuration c) singular configuration of b)

To detect singular configurations in a tensegrity structure, basic methods for singularity detection can be used as a starting point. The inverse kinematic equation for length of tendons as function of the nodal positions has already been presented in Eq.(2.4). To calculate singular configurations, the variation ∂L_{t_i} as a function of ∂p is desired. The derivation is presented in Eq.(3.4).

$$\begin{aligned} \partial L_{t_i} &= \partial \left(p^T C_{t_i}^T C_{t_i} p \right)^{1/2} \\ \partial L_{t_i} &= \frac{1}{L_{t_i}} p^T C_{t_i}^T C_{t_i} \partial p \\ \partial L_{t_i} &= J_{p_i}(p) \partial p \end{aligned} \tag{3.4}$$

In Eq.(3.4) J_{p_i} is a row vector with length $D \cdot 2n_b$, where D has value 2 for 2D and 3 for 3D structures. The topology matric C_{t_i} corresponds to the rows in C_t related to tendon i. When ∂L_{t_i} of all n_t tendons is collected a vector ∂L_t can be formed:

$$\begin{aligned} \partial L_t &= J_p(p) \partial p \\ \begin{bmatrix} \partial L_{t_1} \\ \partial L_{t_2} \\ \vdots \\ \partial L_{t_{n_t}} \end{bmatrix} &= \begin{bmatrix} J_{p_1} \\ J_{p_2} \\ \vdots \\ J_{p_{n_t}} \end{bmatrix} \partial p \end{aligned} \tag{3.5}$$

In Eq.(3.5) $J_p(p)$ is a matrix with dimensions $n_t \times D \cdot 2n_b$.
Looking at the definition for singularities in tensegrity structures, it is logical to check for singularities per bar. It is however difficult to check for singularities with $J_p(p)$, since this Jacobian is not arranged per bar. To accomplish sorting per bar, the Jacobian must be multiplied by the permutation matrix C_{map}, which contains the mapping from the consecutive numbering of nodes per bar p_b to the global numbering of nodes p, as illustrated in Figure 3.3. Eq.(3.6) presents the adjustments to the Jacobian.

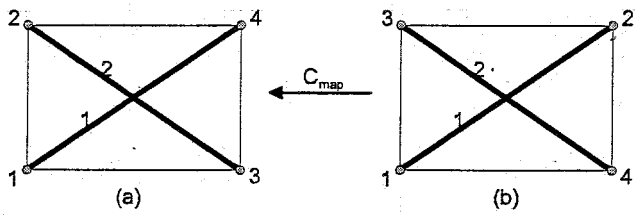

Figure 3.3: a) global numbering of nodes b) consecutive numbering of nodes per bar

$$\partial p = C_{map}\ \partial p_b \quad \text{resulting in} \quad J_{p_b}(p) = J_p(p) C_{map} \tag{3.6}$$

The regular approach for finding the singular configurations is concerned with the rank of the complete Jacobian. This approach cannot be used to check singularity in tensegrity

structures, since in that case, tendons that are *not* connected to a specific bar, *are* included in the manipulability check for that bar. This is not conform the definition of manipulability given in this Subsection. To detect singular configurations in tensegrity structures, $J_{p_b}(p)$ has to be divided into n_b separate matrices of dimension $n_t \times 2D$. Each sub matrix represents the relation between changes in nodal positions of a bar and changes in tendon length of the tendons attached to that bar. The sub matrices all have to have full rank to avoid singularity. When a sub matrix does not have full rank, singularity occurs.
It is possible that not all bars have to be checked for singular configurations, especially when the number of bars in a tensegrity structure increases. The shape of a tensegrity structure is defined by the position of a number of nodes and thus a number of bars (possibly $< n_b$). Manipulability of these bars is relevant, the manipulability of the other bars can be neglected, if desired.
For the design of a reference trajectory, singularities can be taken into account by using one of the presented performance indices. By limiting the permitted values of the applied index, a lower bound for manipulability can be established.
A remark has to be made about the singularity analysis. It looks like singularities and force equilibrium of a tensegrity structure are closely related. Singular situations (often?) occur when a stable equilibrium of the tensegrity structure cannot be guaranteed. If this is always the case, is not known. Future studies should determine the relation between singularities and integrity. If they are equivalent, the singularity constraint can be removed from the reference trajectory generator.

3.2 Collision detection

In different research fields, collision plays an important role. Graphic designers use the idea of bounding boxes to approximate complex shapes [20]. Studying the distance between the boxes gives an good first indication of whether or not two objects collide. If collision is suspected, closer investigation is done to confirm or reject the collision.
When dynamics are involved, not only the collision detection is important, but also reaction forces and deformations of the colliding bodies [21]. With tensegrity structures, the dynamics that occur during a collision are irrelevant; the elements should not collide, no matter what the collision forces are. It suffices to detect collisions between elements.
In order to simplify collision detection, it is assumed that the cross sections of the elements are round and constant over the complete length. This assumption makes bounding boxes superfluous and basic algebra can be applied. Collision detection in tensegrity structures can be summarized by finding the smallest distance between two arbitrary elements. When this distance is smaller than the sum of the two radii of the elements, collision occurs.

In Figure 3.4 two elements are shown. l_1 and l_2 represent arbitrary points on the elements, with l_i equal to zero for $p_{i,1}$ and one for $p_{i,2}$. The vector representation of the distance between two points on the elements is given in Eq.(3.7), with vector t_i defined in Eq.(2.3).

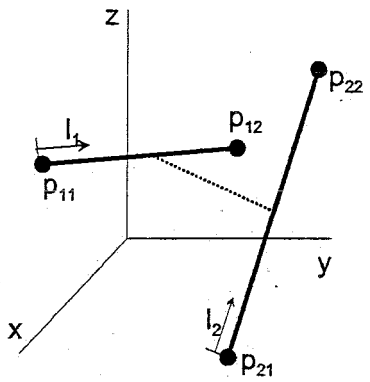

Figure 3.4: Distance between two elements

$$\begin{aligned} t_{dist} &= (p_{2,1} + t_2 l_2) - (p_{1,1} + t_1 l_1) \\ t_{dist} &= Ax + b \\ \text{with } A &= \begin{bmatrix} -t_1 & t_2 \end{bmatrix} \quad , \; x = \begin{bmatrix} l_1 \\ l_2 \end{bmatrix} \quad \text{and} \quad b = \begin{bmatrix} p_{2,1} - p_{1,1} \end{bmatrix} \end{aligned} \tag{3.7}$$

The Euclidean norm of the distance is presented in Eq.(3.8):

$$L_{dist} = ||t_{dist}|| = \left[(Ax + b)^T (Ax + b) \right]^{1/2} \tag{3.8}$$

To find the smallest distance between the lines on which the elements lay, Eq.(3.8) must be differentiated with respect to x and set to zero:

$$\frac{dL_{dist}}{dx} = 0 \rightarrow A^T A x_{min} = A^T b \tag{3.9}$$

Using x_{min} from the solution of Eq.(3.9) in Eq.(3.8) will give the smallest distance between the *lines* on which the two elements lay. This does not guarantee that the points are located on the elements, since x_{min} can be smaller than zero or greater than 1. For parallel situations, it is not possible to directly calculate the smallest distance between the two elements, since Eq.(3.9) only results in one equation. And with one equation, only the ratio between l_1 and l_2 can be found. Two elements lay parallel when $rank(A^T A) = 1$. To find x_{min}, take an arbitrary value for l_1, e.g., 0, and determine l_2.
To find the smallest distance between the two *elements*, two procedures can be followed. The difference between the two is, that the first procedure uses optimization for all possible configurations of two elements, while the second procedure filters out several configurations, before optimization is applied.

The first procedure makes use of a quadratic optimization algorithm. The objective function to be minimized is defined as the square of Eq.(3.8). Solutions for x_{min} should lay between the bounds $0 < LB \leq x_{min} \leq UB < 1$.
Eq.(3.10) summarizes the optimization algorithm.

$$\min_x \frac{1}{2} x^T A^T A x + A^T b x \quad , \text{ sub } LB \leq x \leq UB \tag{3.10}$$

Using x_{min} from Eq.(3.10) in Eq.(3.8) the smallest distance can be determined. If this distance is smaller than the sum of the radii of the two elements $r_1 + r_2$, collision occurs.

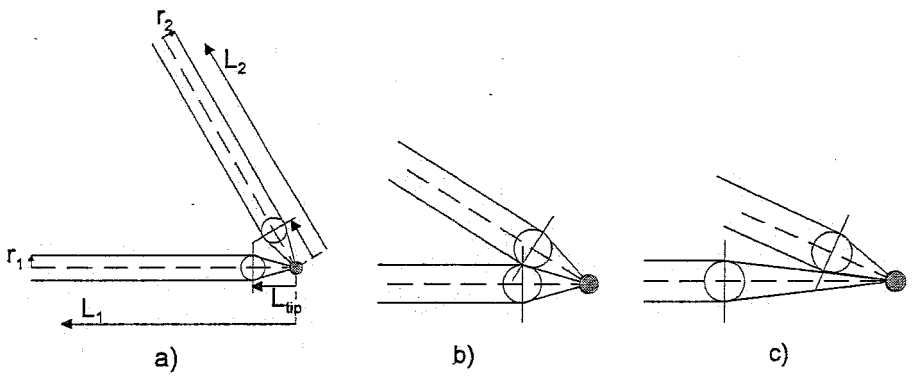

Figure 3.5: a) Connection between two elements, b) Collision between two similar elements, c) Collision between two different elements

The upper and lower bounds are mainly stringent for situations where two bars are connected in one node. Figure 3.5 illustrates the different possible configurations of two connected bars. These situations do not occur in Class 1 tensegrity structures, since no two bars are directly connected. The values for LB and UB can therefor be very close to zero and one respectively. The bounds cannot equal zero or one, since two connected elements will than always collide, assuming nonzero radii of the elements in the node.

The second procedure that can be followed is by systematically passing through a number of steps to exclude the possibility of collision. The procedure contains the following steps:

1. Looking at examples at [2], tendons at the end of a bar can touch the bar at other positions than the node. Two situations are presented in Figure 3.6. It is however decided that the collision in Figure 3.6 b) is allowed to happen. Two elements, connected to the same node, can therefor be removed from the procedure. The possibility that this situation actually occurs, is relatively small. When tendons are positioned as in Figure 3.6 b), the forces in the tendons are probably quite large and force constraints will not allow that to happen (as will be seen in Section 3.3).

2. The second step determines whether or not two elements are close enough to be able to collide. Possibly two elements are so far apart, that collision is impossible to occur. When at least one of the four possibilities of Eq.(3.11) is true, there will be no collision.

Figure 3.6: a) no collision between the bar and tendon, b) allowed collision between a bar and tendon

$$||p_{2,j} - p_{1,i}|| \geq L_1 + L_2 \quad \text{for } i = [1,2] \text{ and } j = [1,2] \tag{3.11}$$

3. It is possible that two elements lay parallel. With l_1 equal to some arbitrary value, e.g., 0, the value of l_2 can be determined. With l_1 and l_2 the smallest distance can be calculated and collision can be predicted.

4. This step requires the smallest distance between the lines on which the elements lay. It is of no concern whether or not x_{min} satisfies the constraints of the lower and upper bounds. If the smallest distance is larger than the sum of the radii of the elements, no collision occurs.

5. If non of the above steps exclude collision, the quadratic optimization has to be performed. From this a final statement about collision can be made.

Since the total number of collision checks, $N_{collision}$, equals:

$$N_{collision} = \sum_{i=1}^{n_t+n_b-1} i = \frac{(n_t+n_b)\left((n_t+n_b)-1\right)}{2},$$

for larger tensegrity structures the second procedure can save computation time. Hereby it is assumed that optimization is computational more demanding than basic algebraic calculations. A combination of the two procedures can also be applied, e.g., first step one of the second procedures is carried out and immediately after this, optimization is applied. It must be mentioned that this way of collision detection does not work properly when the steps in the shape change are too large. As an example assume the next situation: at one step, a bar is left of another bar and in the next step the same bar is on the right of that other bar. In both steps no collision has been detected, while between the two steps the bars moved through each other. Therefor, when there are doubts about collisions, it can be wise to do an extra check during a simulation of the shape change. By visualizing the shape change, possible collisions can be seen. When there are still doubts, a small time period around a possible collision can be selected. By decreasing the time steps in the simulation and continuously (at every time step) calculating the smallest distance between the two, possibly colliding, elements, collision can be confirmed or rejected.

3.3 Force constraints

The force constraints are preceded by an integrity check. This integrity check is nothing more than determining the element forces in the tensegrity structure, as discussed in Section 2.4. In the design of the reference trajectory, stable equilibria of a tensegrity structure during and after the shape change are desired, i.e., integrity checks must result in feasible solutions. The output of the optimization algorithm for integrity provides the element forces and a feasibility index. When a solution is feasible, the index will be 1 or 2. Otherwise the index is smaller than or equal to zero. The feasibility constraint can thus be summarized as: $-feasibility + 1 \leq 0$. Besides the fact that integrity is checked, the element forces are also directly determined.
Constraints related to the forces in a tensegrity structure are found in the fact that tendons do not have an infinite tensile strength and bars are not allowed to be subjected to forces larger than the Buckling force or the compressive yield force. These constraints are presented in Eq.(3.12), Eq.(3.13), and Eq.(3.14).

$$F_{max,yield} = A_t \sigma_{yield} \quad \rightarrow \quad F_t^* - \kappa F_{max,yield} \leq 0 \tag{3.12}$$

$$F_{min,buckling} = \frac{-\pi^2 EI}{L_b^2} \quad \rightarrow \quad \kappa F_{min,buckling} - F_b^* \leq 0 \tag{3.13}$$

$$F_{min,yield} = -A_b \sigma_{yield} \quad \rightarrow \quad \kappa F_{min,yield} - F_b^* \leq 0 \tag{3.14}$$

In Eq.(3.12) A_t and A_b are the cross sectional area of respectively a tendon and a bar and σ_{yield} is the yield stress of the material used for the elements. In Eq.(3.13) I is the second moment of area of a bar about the neutral axis. The κ is introduced into the equations as a safety factor, with $0 < \kappa \leq 1$.
The Buckling force and negative yield force can be calculated on forehand. Only the constraint related to the smallest negative force has to be taken into account in the final optimization algorithm, since that is the most stringent constraint.
A final constraint describes the maximum allowed force change between two steps in the shape change:

$$\left(F_k^* - F_{k-1}^*\right) - \Delta F \leq 0, \quad -\Delta F - \left(F_k^* - F_{k-1}^*\right) \leq 0 \tag{3.15}$$

This constraint makes sure that forces in the elements do not change too rapidly, since this could cause unexpected dynamic behavior of the tensegrity structure and possibly damage of one of the elements.

3.4 Design of the reference trajectory

In Sections 3.1, 3.2, and 3.3 the most important constraints for shape control are defined. However, before the final reference trajectory can be designed, there are a some other constraints that have to be mentioned. These constraints are presented in Subsection 3.4.1. When all the constraints are gathered, the optimization objective is presented in Subsection 3.4.2.

As is shown in Chapter 2, a tensegrity structure can be defined with several variables. This means that the reference trajectory can be determined by optimizing different variables. The benefits and drawbacks of the use of these variables are discussed in Subsection 3.4.3. Finally, a complete summary of the reference trajectory is given in Subsection 3.4.4.

3.4.1 Extra constraints

Some nodes in a tensegrity structure will be fixed to the ground, e.g., by joints. These joints will remove one or more DOFs of a node. In the optimization algorithm there has to be a constraint that represents the effect of the joints. In Eq.(3.16) the result of the linear constraint is presented.

$$A_{eq_J} p = p_{joint} \tag{3.16}$$

In Eq.(3.16) p_{joint} is the vector with the joint positions. Matrix A_{eq_J} connects the fixed nodal positions to the joint positions, so that the fixed nodal positions have the same values as p_{joint}.
In order to perform a shape change, a shape has to be defined. This can be done by prescribing the actual position of one or more nodes. It can also be preferred that one or more node coordinates are a function of the other coordinate(s). This way, a node can be placed on a trajectory described by any function, without prior knowledge of the exact final position of the node. When an actual position is prescribed, Eq.(3.16) can be used with $p_{position}$ and A_{eqp} instead of p_{joint} and A_{eq_J}. In Eq.(3.17) the nonlinear constraint for shapes is given.

$$f(p_x, p_y, p_z) = 0 \tag{3.17}$$

A third constraint is related to the length of bars. The assumption is that the bars are infinitively stiff, which results in a constant bar length L_b throughout the shape change:

$$L_b - L_{b_0} = ||t_b|| - L_{b_0} = 0 \tag{3.18}$$

A practical constraint is found in the minimum length of the tendons. In theory, the length of a tendon can be zero, but in reality, this will not be possible. Two nodes cannot overlap and zero length of tendons will give numerical problems. Therefor Eq.(3.19) is introduced.

$$L_{t_{min}} - L_t \leq 0 \tag{3.19}$$

Finally, symmetry in the structure can be used to reduce the number of optimization parameters that have to be optimized, i.e., eliminate a number of design variables related to symmetry.

3.4.2 Optimization objective

The objective of the optimization is not determined on forehand. It could be that manipulability is of great importance. This results in optimizing the singularity index of the

tensegrity structure. It can also be the case that the control effort should be as small as possible. The objective function will than be related to the length changes of the tendons. A third objective can be to minimize the forces or force changes in the elements. Perhaps all three objective are important and the objective function contains all three goals.
In this report the decision has been made to optimize the control effort. The corresponding objective function J is presented in Eq.(3.20). The objective is to alter the shape of the tensegrity structure with minimum changes in the tendon lengths.

$$J = \sum_{i=1}^{N_{step}} (L_{t_i} - L_{t_{i-1}})^T (L_{t_i} - L_{t_{i-1}}) \tag{3.20}$$

In the objective function N_{step} denotes the number of shape steps between the initial shape to the final shape.

3.4.3 Optimization variables

The geometry of a tensegrity structure can be expressed by general coordinates, length of elements and nodal positions. Thus the design variables to be optimized in the optimization algorithm can also be different, as illustrated by Figure 3.7.

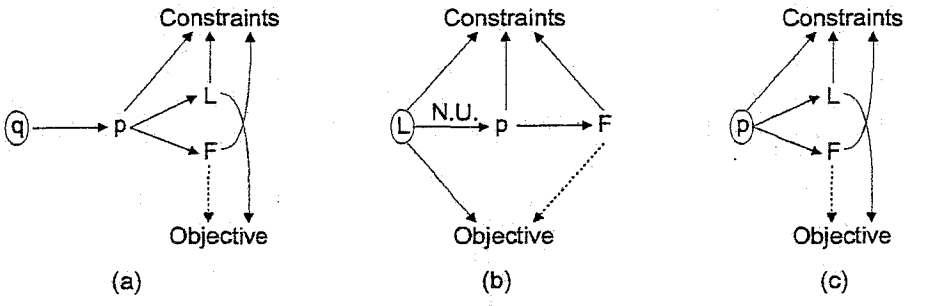

Figure 3.7: a) optimizing q, b) optimizing L (N.U.: Not Unique), c) optimizing p

It is decided to optimize geometric variables only. The element forces are found using statics, described in Section 2.4. It is desired to keep the optimization as simple as possible, i.e., try to describe many (or all) constraints by linear equations. The reason for this, is that the optimization will than be faster and more reliable. The optimization variable that results in the least complex optimization problem will be selected as *the* optimization variable. The three possible geometric variables are discussed briefly.
When generalized coordinates are used, the variables will contain positions of the centers of mass and the Euler Angles of the bars. Since the constraints are expressed in element lengths, nodal positions and forces, kinematic relations between q and p, p and L, and between p and F will have to be applied. All the constraints will be nonlinear.
When the length of tendons and bars are used as optimization variable, the constraints concerned with the element lengths are linear, but the joint and shape constraints require

a mapping from L to p and from p to F. The main problem is that the mapping from L to p does not have to be unique. This can result in false solutions of the optimization.
The variable that remains is p. The joint and position constraints are linear and the kinematic relation from p to L is straight forward and unique. Optimization with nodal positions results in the least complex constraints. Therefor, the nodal positions are used as the optimization variable.

3.4.4 Summary reference trajectory

This Subsection presents the optimization algorithm, with the objective function and all the constraints.

Objective function:

$$\min_{p} \sum_{i=1}^{N_{step}} \left(L_{t_i} - L_{t_{i-1}}\right)^T \left(L_{t_i} - L_{t_{i-1}}\right) \quad \text{Eq.(3.20)}$$

Subject to the equality constraints:

$$\begin{aligned}
A_{eq_J} p - p_{joint} &= 0 && \text{joints, Eq.(3.16)} \\
A_{eq_P} p - p_{position} &= 0 && \text{desired position} \\
f(p_x, p_y, p_z) &= 0 && \text{shape, Eq.(3.17)} \\
||t_b|| - L_{b_0} &= 0 && \text{constant rest length of bars, Eq.(3.18)}
\end{aligned}$$

And inequality constraints:

$$\begin{aligned}
-feasibility + 1 &\leq 0 && \text{integrity/statics, Eq.(2.58) and Eq.(2.59)} \\
Cond.No. - \frac{\max\left(\sigma(J_i)\right)}{\min\left(\sigma(J_i)\right)} &\leq 0 && \text{manipulability, Section 3.1} \\
r_1 + r_2 - ||\left(p_{2,1} + t_2 l_2\right) - \left(p_{1,1} + t_1 l_1\right)|| &\leq 0 && \text{collision, Section 3.2} \\
L_{t_{min}} - L_t &\leq 0 && \text{minimum tendon length, Eq.(3.19)} \\
F_t^* - \kappa F_{max,yield} &\leq 0 && \text{maximum tensile force, Eq.(3.12)} \\
\kappa F_{min,buckling} - F_b^* &\leq 0 && \text{buckling force, Eq.(3.13)} \\
\kappa F_{min,yield} - F_b^* &\leq 0 && \text{maximum compressive force, Eq.(3.14)} \\
\left(F_k^* - F_{k-1}^*\right) - \Delta F &\leq 0 && \text{maximum force change, Eq.(3.15)} \\
-\Delta F - \left(F_k^* - F_{k-1}^*\right) &\leq 0 && \text{minimum force change, Eq.(3.15)}
\end{aligned}$$

The output of the optimization algorithm contains the nodal positions at each step during the shape change. With these nodal positions the length of the tendons L_t during the shape change can be determined, using Eq.(2.3) and Eq.(2.4).

From the nodal positions, the forces in the tendons can be determined, using the statics. With the stressed tendon lengths L_t and the magnitudes of the tendon forces F_t^* the rest length of the tendons can be determined, using Eq.(3.21).

$$L_{t_0} = \frac{L_t}{1 + \frac{F_t^*}{EA_t}} \tag{3.21}$$

In the rest of this report, the reference signals are labelled with the subscript $(\cdot)_{ref}$. With p_{ref}, $F_{t_{ref}}$, and $L_{t_{0_{ref}}}$, all the relevant reference signals for the shape change are determined. To simplify a notation: the tendon force vector $F_{t_{ref}}$ contains the *magnitude* of the forces.

Chapter 4

Control design

In order to find a controller, multiple aspects of control design have to be studied. This Chapter presents the different steps taken. Section 4.1 presents several control strategies, after which one control strategy is selected. Design of the controller is discussed in Section 4.2. In Subsection 4.2.1 a linearized model of the nonlinear dynamics of a tensegrity structure is derived. The different issues related to the design of the controller are worked out in Subsection 4.2.2.

4.1 Control strategies

The goal of the controller is to track the reference trajectory, designed in Chapter 3. Furthermore it is undesired that tendons go slack during and after the shape change and structural vibrations and disturbances should be suppressed. With these specifications in mind, different control strategies are evaluated.

- Feedback Linearization

  A way to deal with the nonlinearities in the dynamics of a tensegrity structure is to apply feedback linearization, [7] and [8]. This methodology transforms the nonlinear system to a linear system, after which linear control strategies can be used to complete the control. Although this method can make the control design a lot easier, it usually requires full state measurements or observers for state reconstruction. In tensegrity structures it is very difficult to measure the generalized coordinates and their time derivatives. And even if this would be possible, it would probably be very expensive. Therefor feedback linearization is not very practical in use for tensegrity structures. The situation where observers are used for state reconstruction, is not further investigated.

- Model Predictive Control

  Model Predictive Control (MPC) is a control strategy that uses predictions of future behavior of the model to determine the next control action. A huge advantage of MPC is that it can handle constraints. For tensegrity structures this means that tension

in the tendons can be guaranteed, as long as the control specifications are not too stringent. MPC uses an optimization algorithm to determine the control output. For larger systems MPC is rather computationally demanding and therefor only useful for relatively slow systems. This drawback makes MPC unsuitable for the control of a tensegrity structure in this report, since the shape changes will be carried out in relatively short times and the tensegrity structure can be a fast system, due to possibly high stiffness of the structure.

- Neural Network

  One of the proposed controllers in [8] is a neural network. The network is used as an open loop tracking controller. As seen in Section 3.1, a redundant system like a tensegrity structure, is not kinematic invertible. All the neural network does, is finding a path that approximates the pseudo inverse kinematics. It is thus used for function approximation. The reference trajectory generator from Chapter 3 already provided a path and thus neural networks are of no use in this research.

- Gain Scheduling Control

  During a shape change the reference generator determines several operating points. At each operating point a linear model of the tensegrity structure can be obtained. To design a Gain Scheduling Controller, all the linearized models have to be parameterized by one or more scheduling variables. Then parameterized linear controllers can be designed that ensure some level of performance at each operating point. This control strategy sounds promising, but too little time is available to work it out.

- $\mathcal{H}_\infty$, $\mathcal{H}_2$ Control, and Pole Placement

  Pole placement can be an effective way to add damping to the system. This can be very beneficial for tensegrity structures made from material with little damping. It is up to the designer to define a desired region in which the closed loop poles must lay. Using Linear Matrix Inequalities (LMI's) a controller can be found (for background information on LMI's, see [22]). The controller found with pole placement does not give any guarantees about performance or robustness of the closed loop system. Therefor $\mathcal{H}_\infty$ and $\mathcal{H}_2$ control is introduced.

  A common used control strategy is linear $\mathcal{H}_\infty$ control. This controller ensures some level of performance and guarantees stability in a region around the operating point. The $\mathcal{H}_\infty$ controller is obtained by minimizing the maximum singular value of weighted closed loop transfer functions related to performance and robustness. Mathematically this can be done by using an optimization algorithm, or by solving LMI's. In [9] two $\mathcal{H}_\infty$ controllers are used for the deployment of a tensegrity structure.

  An $\mathcal{H}_2$ controller has many similarities with the $\mathcal{H}_\infty$ controller. The main difference is that $\mathcal{H}_2$ minimizes the squared singular values over the complete frequency range, while $\mathcal{H}_\infty$ just minimizes the maximum singular value. The objective can be compared with minimizing the output energy, related to impulses on the inputs. Using $\mathcal{H}_2$ instead of $\mathcal{H}_\infty$, makes robustness subordinate to reduction of output energy. The optimal $\mathcal{H}_2$ controller follows from solving a Riccati equation or from solving LMI's.

The beauty of LMI's is, that several control objectives can be combined into one (sub-optimal) control design. The benefit of this is, that performance and robustness can be obtained together with some level of damping.

After the evaluation of the mentioned control strategies it has been decided to work with an $\mathcal{H}_2$ controller with pole placement. Pole placement guarantees some level of damping in the system, while an $\mathcal{H}_2$ controller sets a lower bound on performance. The aspect of energy reduction of output signals makes $\mathcal{H}_2$ preferable over $\mathcal{H}_\infty$, because it focusses on minimizing the control objectives (energy) over the complete frequency spectrum, instead of focussing only on one frequency, which is the case with $\mathcal{H}_\infty$ control.

4.2 Controller design

Aspects of the $\mathcal{H}_2$ control design are worked out in this Section. In Subsection 4.2.1 a linear model of the nonlinear dynamics is derived. Issues related to the actual control design are presented in Subsection 4.2.2.

4.2.1 Linearization

To be able to apply linear control strategies to a tensegrity structure, the dynamics of the system should be linearized. The obtained model is presented in state space representation, illustrated by Eq.(4.1). Linearization must be done around a stable equilibrium of the nonlinear system. This equilibrium situation is represented by $x(0)$ and $u(0)$.

$$\begin{aligned} \dot{\tilde{x}} &= A_p\tilde{x} + B_p\tilde{u} \\ \tilde{y} &= C_p\tilde{x} + D_p\tilde{u} \\ \text{with } \tilde{x} &= x - x(0) \text{ and } \tilde{u} = u - u(0) \end{aligned} \tag{4.1}$$

Linearization by means of numerical differentiation of the nonlinear system results in relative errors in the linearized model in the order of $\sqrt{\varepsilon}$, with ε the machine accuracy. To obtain a precise linearization, the toolbox MAD (Matlab Automatic Differentiation) [23] is applied. This toolbox uses operator overloading to simultaneously determine the outcome of a function or operator, together with the derivative with respect to the input signals. The outcome has a relative error of $O(\varepsilon)$.

The nonlinear dynamics of a Class 1 tensegrity structure can be described by Eq.(4.2). Instead of using all generalized coordinates, the q's related to restricted directions are left out. In the formulation of the nonlinear dynamics in Subsection 2.3.3 this has also been done: the force equations related to restricted directions were removed.

$$\begin{gathered} \dot{x}_{nl} = f_{nl}(x_{nl}, u)\ , \quad y = g_{nl}(x_{nl}, u) \\ \text{with } x_{nl} = \begin{bmatrix} q_{nl}^T & \dot{q}_{nl}^T \end{bmatrix}^T \end{gathered} \tag{4.2}$$

The input into the system is given by u and represents the rest length of the tendons. The output y equals the generalized coordinates without the restricted directions: q_{nl}.
Normally the Jacobian of f_{nl} and g_{nl} with respect to x_{nl} and u is taken to obtain the state space matrices of the linearized model. Unfortunately this straight forward derivation cannot be applied to dynamics described with Euler parameters: Euler parameters are dependent, since their length equals one: $e_0^2 + e_1^2 + e_2^2 + e_3^2 = 1$. When the linearization is carried out with dependent states, the linear model will not be observable and controllable. This is because the dependency is not accounted for.
A minimal linear representation of the nonlinear dynamics, including the dependent states, can be obtained. First, rounding errors ($\leq O(10^{-12})$) during the linearization, resulting in small positive real parts of the eigenvalues $Re(\lambda(A_p))$, must be moved to the left half plane. A solution for this problem is presented in [24]: $A_{p,new} = A_p - (max(Re(\lambda(A_p))) + \epsilon)I$, with ϵ a very small positive number. Second, the linearized system must be balanced and model reduction must be applied. Per bar two states, with the smallest Hankel Singular Values, have to be removed: the first and second time derivative of the Euler parameters both have a dependent Euler parameter.
However, this method is not preferred, since the final answer is obtained merely by applying "tricks". A decent way to obtain a minimum number of independent states x is presented in the next paragraphs and deals with proper removal of the redundant states.

A way to remove the dependency is to write one Euler parameter as a function of the others. Solving the quadratic equation for Euler parameters for one parameter results in an expression with a square root. Taking the square root of a number can result in a positive as well as a negative value. It is not clear on forehand which sign to take.
To solve this problem of the unknown sign, the Tait-Bryant Angles are reintroduced. The rotation around the local z-axis is defined for $-\pi/2 \leq \theta \leq \pi/2$, while around the local y-axis, the angle is defined for $0 \leq \varphi \leq 2\pi$. The Euler parameters are presented again in Eq.(4.3).

$$\begin{bmatrix} e_0 \\ e_1 \\ e_2 \\ e_3 \end{bmatrix} = \begin{bmatrix} \cos\left(\frac{\theta}{2}\right)\cos\left(\frac{\varphi}{2}\right) \\ -\sin\left(\frac{\theta}{2}\right)\sin\left(\frac{\varphi}{2}\right) \\ \cos\left(\frac{\theta}{2}\right)\sin\left(\frac{\varphi}{2}\right) \\ \sin\left(\frac{\theta}{2}\right)\cos\left(\frac{\varphi}{2}\right) \end{bmatrix} \tag{4.3}$$

Using the range of the Tait-Bryant Angles, it can be seen that $\cos(\theta/2) \geq 0$ and $\sin(\varphi/2) \geq 0$. Since e_2 is defined as $\cos(\theta/2)\sin(\varphi/2)$, its value will always be greater than or equal to zero. The dependency in the Euler parameters can thus be removed by rewriting e_2 as a function of the others.
Figure 4.1 schematically illustrates the mappings from the initial generalized coordinates, to the generalized coordinates used in the nonlinear model, and to the minimum number of generalized coordinates.

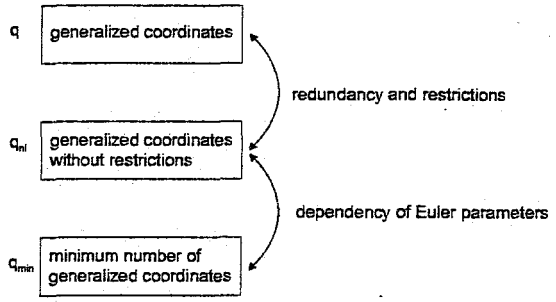

Figure 4.1: Mappings from top to bottom q, q_{nl} and q_{min}

For the 2D case some Euler parameters are redundant. This makes it not always possible to write e_2 as a function of the other parameters, since in some 2D situations e_2 always equals zero. Dependency has than been looked for in another Euler parameter. In Table 4.1 the final results for redundancy and dependency are presented in the second and third row respectively.

Table 4.1: Combining Tait-Bryant Angles and Euler parameters

	3D	$X-Y$ $(\varphi=0)$	$X-Z$ $(\theta=0)$	$Y-Z$ $(\theta=\pi/2)$
red.		$q_z=0$ $e_1=0$ $e_2=0$	$q_y=0$ $e_1=0$ $e_3=0$	$q_x=0$ $e_1=-e_2$ $e_0=e_3$
dep.	$e_2=+\sqrt{1-e_0^2-e_1^2-e_3^2}$	$e_0=+\sqrt{1-e_3^2}$	$e_2=+\sqrt{1-e_0^2}$	$e_2=+\sqrt{1/2-e_0^2}$

The minimum number of independent states is defined as $x=[q_{min}^T \ \dot{q}_{min}^T]^T$. The A_p, B_p, C_p and D_p matrices can be found using Eq.(4.4).

$$A_p=\frac{\partial f_{nl}}{\partial x_{nl}}\frac{\partial x_{nl}}{\partial x}\ ,\ B_p=\frac{\partial f_{nl}}{\partial u}\ ,\ C_p=\frac{\partial g_{nl}}{\partial x_{nl}}\frac{\partial x_{nl}}{\partial x}\ ,\ D_p=\frac{\partial g_{nl}}{\partial u}=0 \tag{4.4}$$

Initially y is chosen to be equal to q_{min}, resulting in $C_p=[I;0]$. However, it can also be desired to have the nodal positions, tendon lengths or even the tendon forces as the output of the linearized model. Remember therefor from Subsection 2.2.3 that $p=f_{pq}(q)$ and $L_t=f_{L_tp}(p)$. Given Eq.(2.15), the tendon forces can be determined. Note that for a static situation the forces are only a function of the stressed tendon lengths L_t and rest lengths L_{t_0}. In short notation this is rewritten to $F_t=f_{FL}(L_t,u)$, with u the rest length of the tendons. Although damping is not present in the static mapping from q_{min} to F, it is already present in A_p (when $d_{damp}>0$). The different C and D matrices can be found using Eq.(4.5), Eq.(4.6) and Eq.(4.7).

$$C_{p_p} = \frac{\partial f_{pq}(q)}{\partial q} C_p, \quad D_{p_p} = 0 \tag{4.5}$$

$$C_{p_{L_t}} = \frac{\partial f_{L_t p}(p)}{\partial p} \frac{\partial f_{pq}(q)}{\partial q} C_p, \quad D_{p_{L_t}} = 0 \tag{4.6}$$

$$C_{p_F} = \frac{\partial f_{FL}(L_t, u)}{\partial L_t} \frac{\partial f_{L_t p}(p)}{\partial p} \frac{\partial f_{pq}(q)}{\partial q} C_p, \quad D_{p_F} = \frac{\partial f_{FL}(L_t, u)}{\partial u} \tag{4.7}$$

Using A_p , B_p , C_{p_i} and D_{p_i} a linearized model is defined with one of the four possible outputs. Combination of different outputs is also possible. If for example both nodal positions and tendon forces are desired as outputs, the C and D matrices become $[C_{p_p}; C_{p_F}]$ and $[D_{p_p}; D_{p_F}]$.
A final remark, the linearized model deals with variations in the inputs and outputs around a stable operating point. Design of a controller, using the linearized model, will thus only result in variations of the input signal of the nonlinear system around stable equilibrium situations.

4.2.2 $\mathcal{H}_2$ control

Before going into detail about the design of an $\mathcal{H}_2$ controller, an overall picture of the complete control scheme is presented. The feedback controller will be designed with a linearized model of the nonlinear system. Therefor the inputs of the controller must contain the variations of the reference signals and measurements around an equilibrium situation, as seen in Eq.(4.1). The output of the controller corresponds to variations on the input signal of the nonlinear system. The actual shape change is the result of the feedforward signal. A general closed loop system with a 2 DOF controller is presented in Figure 4.2. Here, (0) corresponds to the values of the variables in the equilibrium situation.

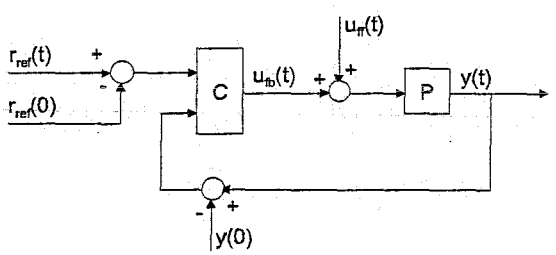

Figure 4.2: Closed loop scheme for (non)linear system with linear feedback control

The values of the different input signals can be obtained from the reference trajectory.

Two basic schemes for a feedback controller are given in Figure 4.3. Though there are more configurations possible, the controller design will be concentrated on these two configurations. Figure 4.3 a) presents a 2 DOF controller, while 4.3 b) presents a 1 DOF controller. Both control schemes can be used for $\mathcal{H}_2$ control, so at this point no decisions are made

about the configuration of the controller. A benefit of a 2 DOF controller is, that during the control design more freedom is given to the optimization algorithm to find optimal input-output relations. A drawback of the 2 DOF controller is the number of inputs into the controller.

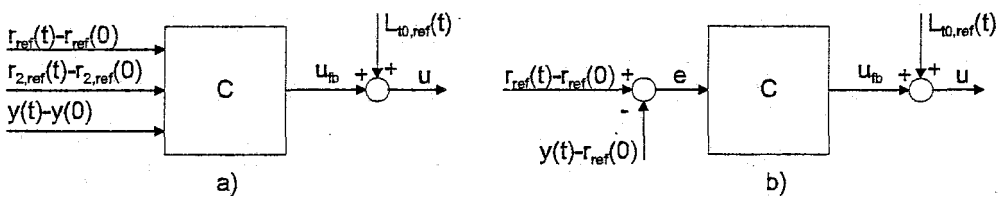

Figure 4.3: a) 2 DOF controller, b) 1 DOF controller

For the design of an $\mathcal{H}_2$ controller a number of questions have to be answered.

- Which variables y will be measured?
- What are the input variables r_{ref} and $r_{2,ref}$ of the system?
- What is the control objective?
- Are there disturbances active in the system and where?
- Which frequencies are relevant in the input and output signals?

A possible measurement variable can be found in generalized coordinates. However, as discussed before, determining the generalized coordinates of bars is very difficult. More obvious variables to measure are nodal positions or stressed tendon lengths. Tendon lengths are easier to determine than nodal positions, but they could give problems with shape control. A shape defined in stressed tendon lengths could result in a wrong configuration of the bars, as seen in Subsection 2.2.3. On forehand it is difficult to determine which variable is best suited for measurements. Possibly simulations could give the answer.
In case of a 1 DOF controller, one input related to desired shape must be present in the control scheme. This shape can best be defined by nodal positions, i.e., $r_{ref} = p_{ref}$; generalized coordinates are not very workable in practice and tendon lengths do not guarantee a unique configuration. When a 2 DOF controller is used, an extra input can be defined. The extra input has to be related to the tension in the tendons. Both the rest length of the tendons $L_{t_{0,ref}}$ as the tendon forces $F_{t_{ref}}$ are suitable, thus the extra input can be $r_{2,ref} = F_{t_{ref}}$ as well as $r_{2,ref} = L_{t_{0,ref}}$.
Possible control objectives in the design of a controller for tensegrity structures can be: good tracking of a shape and avoidance of zero tension in tendons. Disturbance rejection is already an integral part of the previous two objectives. Good tracking is nothing more than minimizing the error between the actual nodal positions and the reference nodal positions. Avoiding slackness of tendons can be translated into minimizing the difference between the actual tendon forces and the reference tendon forces. An extra objective that can

be introduced, is the minimization of the feedback control effort. In this report all three objective are included in the controller design. They are summarized as minimizing $e = p - p_{ref}$, $\Delta F = F_t - F_{t_{ref}}$ and u_{fb}. Note that the control objectives and outputs of the system used for the controller design, are identical.
Different disturbances can be active on a tensegrity structure. There could be friction in the actuators, resulting in a disturbance on the rest length of the tendons. It is also possible that external disturbances work on the bars, resulting in disturbances on the nodal positions. And finally there could be measurement noise. The choice has been made to include actuator friction w, representing Coulomb friction, and measurement noise v in the design of the $\mathcal{H}_2$ controller.
It is common to use weighting filters on the different inputs and outputs, e.g., low pass and high pass filters. Input filters should more or less represent the frequency spectrum or range of the inputs. Output filters should define the frequency region in which the outputs are important for the control design. It can be wise to minimize the complexity of the filters, since the number of states in the final controller will be equal to the states of the linearized model and states of all the filters combined. For tensegrity structures studied in this report, the reference signals are weighted by low pass filters, since no high frequent excitations are present in these inputs. Friction in the actuators is mainly a low frequent phenomenon, therefor w is filtered with a low pass filter. The error objective and tension objective are only important up to some frequency, resulting in low pass filtering. The measurement noise and control effort objective are weighted by high pass filters.

For the design of an $\mathcal{H}_2$ controller, the linearized system and weighting filters must be rewritten to an augmented plant presentation. In Figure 4.4 an augmented plant with a controller C is presented.

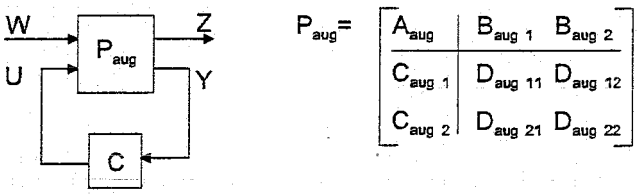

Figure 4.4: Augmented plant

In Figure 4.4 the external inputs into the system are collected in vector W and all the control objectives in output vector Z. The inputs into the controller are gathered in Y and the control outputs in U. For both LMIs and Riccati equations, D_{11} must be zero. When D_{11} is unequal to zero, there is a direct throughput from external inputs to the control objectives and no guarantee can be given about bounds on the energy in the system. Since the control strategy is based on finite energy in the system, no feasible controller can be found. Riccati equations require the extra constraint that D_{12} and D_{21} have to have full row rank, in order to find a solution. To meet the demands, the weighting filters can be chosen to be proper or strictly proper.
Figure 4.5 presents the specific augmented plant P_{aug}, used for the 2 DOF controller. For

this scheme the second reference input $r_{2,ref}$ is defined as the reference force $F_{t_{ref}}$. The measurements y contain the nodal positions p. The V_i and W_i blocks represent the input and output filters respectively. From the inputs of the controller Y, the initial conditions of the variables are subtracted, since the controller is based on variations of variables around an equilibrium. For objectives, this may be done, but it is not necessary, i.e., objectives are not restricted to use variations in variables.

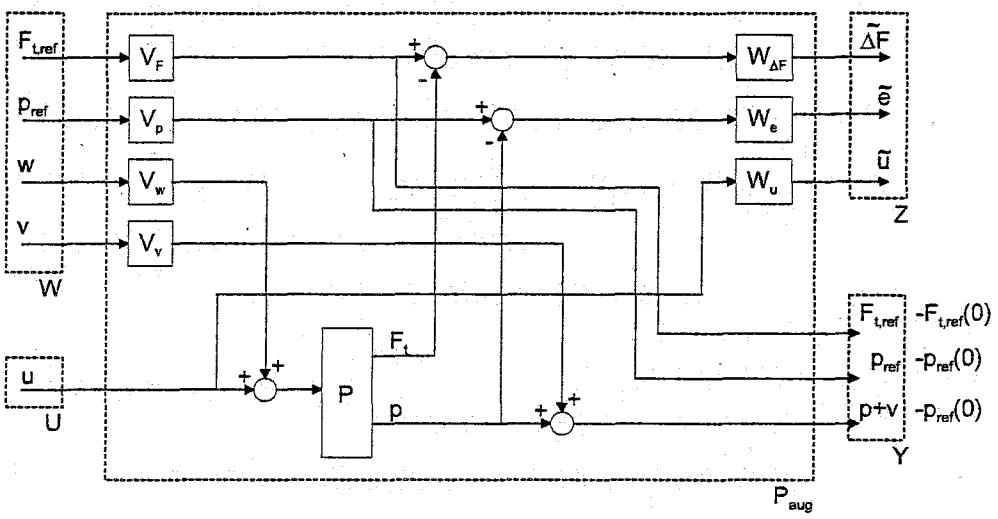

Figure 4.5: Augmented plant for a 2 DOF controller

Chapter 5

2D Example

This Chapter illustrates the theory of the previous Chapters by giving an example of a shape change of a 2D tensegrity structure. The shape change is applied to the structure presented in Figure 5.1. Thin lines represent the tendons, the thick lines are the bars. The desired shape is a second order shape. To remove the rigid body mode, node 2 of the structure is completely fixed to the world and node 1 is restricted in the x direction. Nodes 11 and 12 are not allowed to move in the x direction. Gravity works in the negative y direction. In Appendix A the coordinates of the nodes, the connectivity matrices S_t and S_b and geometric and material properties of the structure are given.

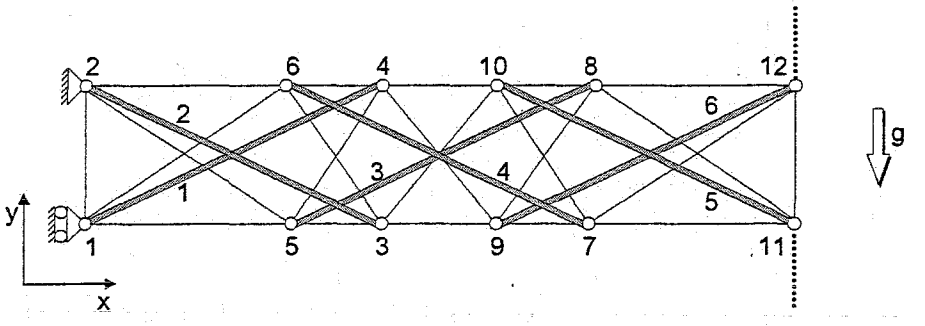

Figure 5.1: 2D tensegrity structure

In Section 5.1 a trajectory is generated and corresponding results are presented. Dynamics related to the shape change and linearization are discussed in 5.2. Finally a controller is designed in Section 5.3 and results are given.

5.1 Trajectory

The shape change of the tensegrity structure is the result of an optimization algorithm with an objective and a number of constraints. The objective has already been discussed in Subsection 3.4.2 and represents the minimum tendon length change during the shape change.

5.1.1 Constraints

Singularities in the 2D tensegrity structure are assumed to be of no importance. It can be seen in Figure 5.1 that no singularities are present in the initial shape and the shape change is expected to be simple enough not to introduce possible singular situations. After the reference trajectory is designed, this assumption is evaluated and if necessary, corrected.
Collision is neglected in this example. The 2D structure is assumed fictional since in the physical world it is not possible for all elements to be in one plane; physical structures will always be three dimensional. To actually build the tensegrity structure in this example, the bars should be curved to avoid collision. In the theoretical 2D structure elements lay over each other and collision occurs constantly. Introducing this constraint for the 2D case would only result in infeasible solutions.
Using the geometric and material properties in Eq.(3.13) and Eq.(3.14) the buckling force is 39 kN and the yield force is 56 kN. Since only the smallest force is needed in the compressive force constraint, yield in the bars can be neglected.
The value for the minimum tendon length is set to $L_{t_{min}} = 0.05$ m. The safety gain κ for the maximum allowed *tensile* forces is set to 0.7 times the yield force of the tendons. The maximum allowed *compressive* forces in the bars is set to 0.7 times the buckling force. For the integrity check a minimum allowed tendon force is defined as 0.06 times the yield force of the tendons. The maximum allowed force change ΔF is set to 10% of the maximum allowed tendon forces. Finally it is assumed that no external disturbances are present in the system.
Constraints related to joints and desired positions are straight forward: the x direction of node 1, 11 and 12 and the x and y direction of node 2 should be kept constant. The bars are considered to be rigid and Eq.(3.18) is applied.
The shape that the tensegrity structure has to follow is a second order shape. In Eq.(5.1) the equations corresponding to the second order shape are given.

$$\begin{array}{ll} y(x) = y_0 & \text{for } x \leq x_0 \\ y(x) = \frac{1}{2}A(x-x_0)^2 + y_0 & \text{for } x_0 < x \leq x_1 \\ y(x) = A(x_1-x_0)(x-x_1) + y(x_1) & \text{for } x_1 < x \leq x_2 \\ y(x) = -\frac{1}{2}A(x-x_2)^2 + A(x_1-x_0)(x-x_2) + y(x_2) & \text{for } x_2 < x \leq x_3 \\ y(x) = y(x_3) & \text{for } x > x_3 \end{array} \tag{5.1}$$

In Eq.(5.1) A is related to the height/depth of the second order shape h by $A = h/((x_1 - x_0)(x_3 - x_1))$. It is chosen to move the shape from the right to the left of the structure with constant "distance" steps, i.e., the horizontal speed of the shape is constant or $x_0(k) = x_0(0) + \Delta x$. In this case Δx is a negative constant, since the shape moves from right to left. In Figure 5.2 the shape and corresponding parameters is plotted.

5.1.2 Reference trajectory results

The results from the reference trajectory generator are presented in Figure 5.3. The actual number of operating points in the shape change, i.e., computed steps in the reference trajectory, is 53, but only 6 steps are presented.

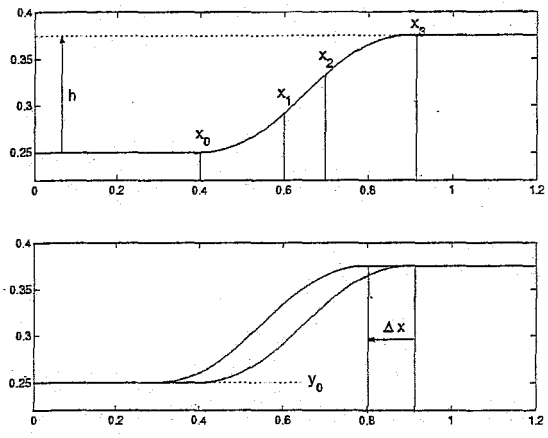

Figure 5.2: Second order shape

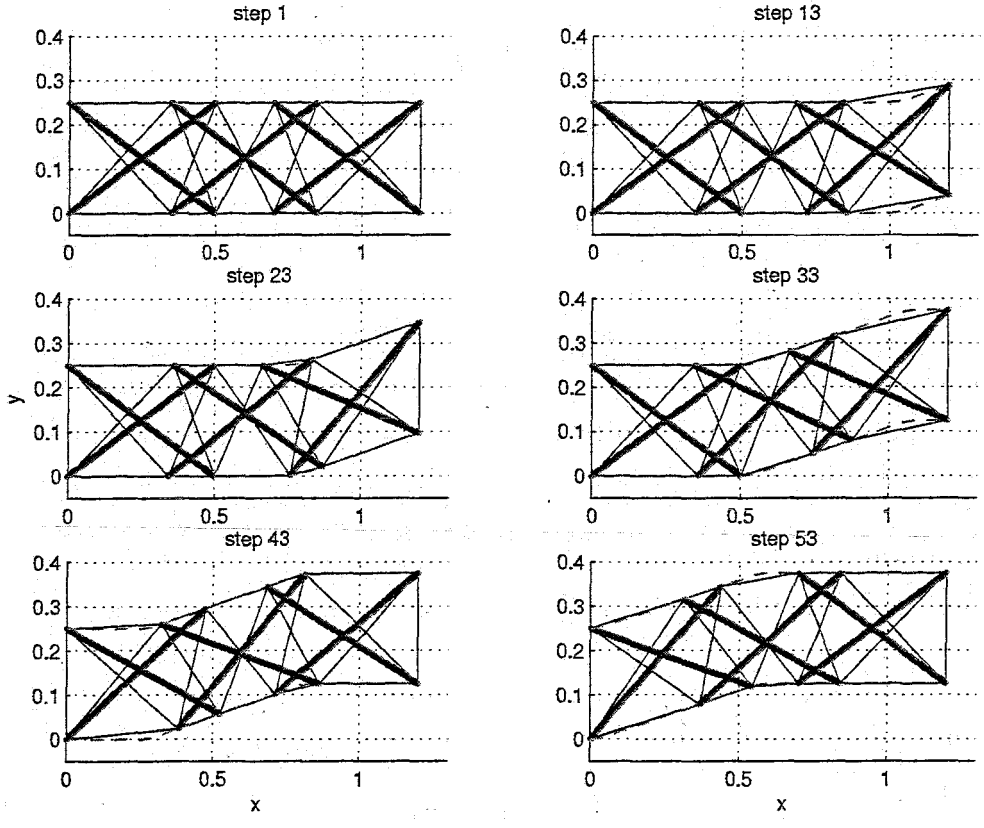

Figure 5.3: Shape change of the tensegrity structure

The dashed lines correspond to the desired shape. As can be seen all the nodes lay on the desired shapes at every step during the shape change. Between the nodes, the tensegrity structure differs in shape from the desired shape. This is caused by the fact that tendons can only connect two nodes by a straight line. The constraints related to restricted directions of the nodes have been dealt with and the bars do not change length. The assumption about singularities has been correct: during and after the shape change, no singularities occur. From this it can be concluded that the reference generator has successfully coped with the corresponding constraints.
To check the force constraints, the static equilibrium forces in the tendons and bars are given in Figure 5.4.

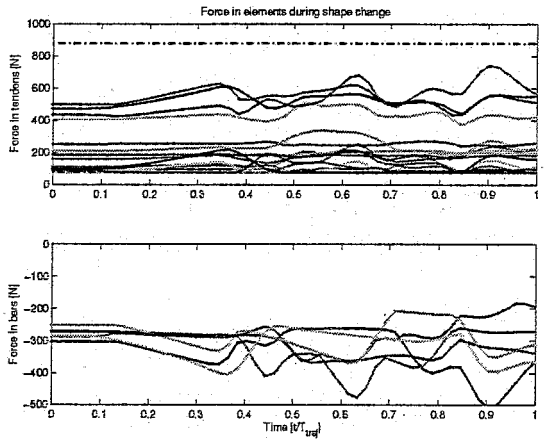

Figure 5.4: Static equilibrium forces in a) tendons and b) bars during shape change

The trajectory time of the shape change is not determined yet. For scaling, the time on the x-axis of the plots is divided by the, yet unknown, trajectory time T_{traj}. Dynamic analysis (Section 5.2) can be used to determine a proper trajectory time. Depending on simulation results, e.g., error signals and pre-stress of tendons, the trajectory time can be increased or decreased.
The dash dotted line indicates the maximum allowed tendon force. It is seen that the tendon forces do not exceed these maximum allowed tendon forces. The bar forces do not even get close to the lower limit of 0.7 times the buckling force.
In Figure 5.4 a) there are four forces that are considerably larger than the other forces. These forces relate to the tendons between the nodes 5-3, 6-4, 9-7 and 10-8, which make up the horizontal connections between the different crosses. Apparently this requires more force. Using another topology of tendons could reduce the difference in tendon force.
From the tendon forces and the nodal positions, the rest length of the tendons can be determined, (Eq.(3.21)). Figure 5.5 shows the rest length of the tendons.
Finally the elongation of the tendons is presented in Figure 5.6. The trajectory of the elongation is again related to the forces in the tendons. Note that the elongation is very small ($O(10^{-4})$) compared to the rest length of the tendons ($O(10^{-1})$), due to the high

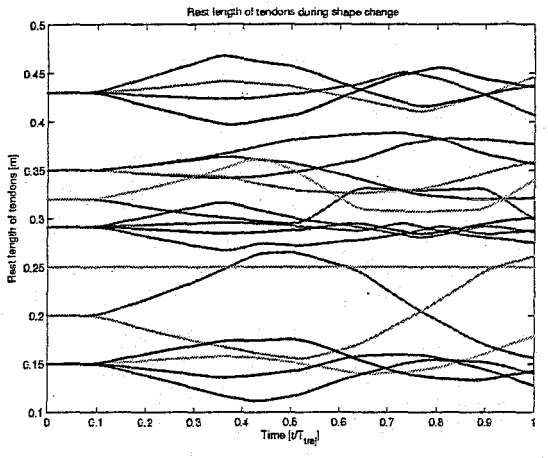

Figure 5.5: Rest length of tendons during shape change

stiffness of the material used for the tendons.

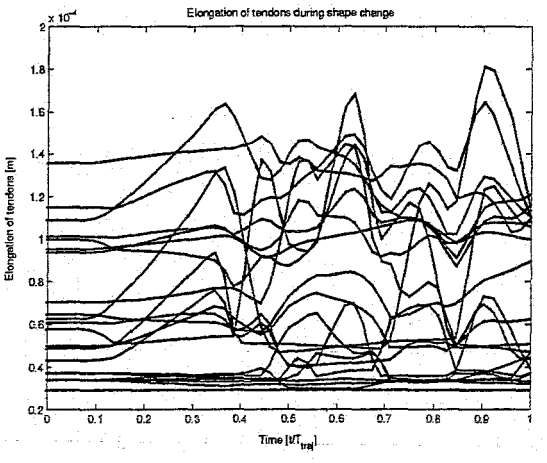

Figure 5.6: Elongation of the tendons during shape change (y axis x10^{-4})

5.1.3 Evaluation

The reference trajectory, presented in this Section, satisfies all constraints. However, since it is a complex optimization problem, it is not certain that the global minimum of the objective is reached. It can neither be confirmed that local (between two steps) minimization of the total change in tendon length results in global minimization (between begin and end shape). The results do look promising, and the shape change does not result in strange configurations of the structure. It is therefor expected that the reference trajectory can be used on an experimental set-up. It is, however, possible that other, or extra, constraints must be

introduced or that constraints must be less stringent. To simplify an experimental set-up, the number of actuators, i.e., active tendons, could be reduced. In this example all twenty-two tendons are active. Passive tendons can be included in the optimization algorithm as extra constraints. In [25] the issue of input/output selection has been discussed.

5.2 Dynamics

5.2.1 Matlab versus Adams

To check if the nonlinear model is correct, in Matlab several simulations have been done with the system, using a 2D single cross tensegrity structure. In the simulations, the number of restricted nodal directions have been varied as well as the magnitude of steps in rest length of one or more tendons. These simulations have been compared to simulations done in the multi-body package Adams. In simulations where nodes are completely fixed, Adams and Matlab show great resemblance. In simulations where a node has only been fixed in one direction, Adams showed small differences in the frequencies present in the output signals (nodal positions), especially in higher frequencies. For all simulations the eigen frequencies and damping of the system were equal.
In [9], accuracy of the solver and the presence of drift in Adams have been studied. Conclusions have been that drift is present in Adams and that the accuracy settings of the solver have a big influence on the simulation results. This could explain the small differences between Adams and Matlab.
Drift in the Matlab model presented in Chapter 2, can occur when errors in simulations alter the length of the Euler parameters. Though it is no proof, for a simple single 2D cross after 40 seconds of simulation, errors in the lengths of the Euler parameters do not exceed $O(10^{-11})$, even when relative accuracy is set to $O(10^{-3})$. Higher accuracies result in even smaller errors.
For simulations of 1.5 seconds with the 2D tensegrity structure of Figure 5.1, the errors in lengths do not exceed $O(10^{-7})$ (relative accuracy of 10^{-3}). The derivatives in lengths of the Euler parameters (fourth equation in Eq.(2.18)) are not equal to zero, but oscillate randomly around zero with amplitudes smaller than (10^{-4}). In this Chapter, simulations never exceed 1.5 seconds. Illustrated by the simulations, the occurrence of drift in the Matlab simulations is not detectable in the selected time span.
In Figure 5.7, the power spectra of two simulations are presented. The plots give the spectra of the horizontal and vertical displacement of a node, for both Adams and Matlab. Other simulations gave similar results. It can be seen that responses from adams and Matlab give (almost) similar power spectra.
From Figure 5.7 the conclusion is drawn that the nonlinear dynamics derived in Section 2.3 are correct and can be used for dynamic analysis of the 2D tensegrity structure.

5.2.2 Feedforward control

Looking at the shape change and simulation results, a trajectory time of 1 second looks reasonable. Initially, the rest length of the tendons, $L_{t_{0_{ref}}}$, is used as the feedforward signal

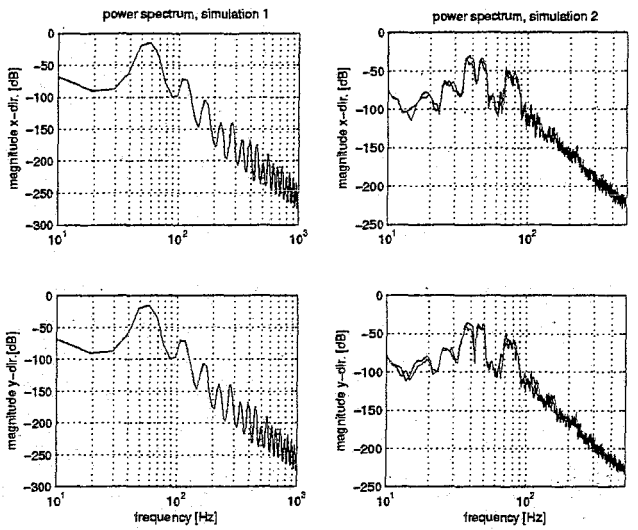

Figure 5.7: Comparison between power spectra of Matlab responses and Adams responses

for the nonlinear dynamics of the 2D tensegrity structure, since these rest lengths can be changed actively by actuators. The outputs of the system are chosen to be the errors in nodal positions and the elongation of the tendons. To obtain the errors in nodal position, a second input signal, p_{ref}, is needed in the system.
In simulations, the reference signals between two operating points are obtained through linear interpolation. The use of $L_{t0_{ref}}$ as input signal results in a dramatic decrease of tension in the tendons between two operating points. This is checked by using $F_t = EA_t/L_{t0_{ref}}(L_t(p_{ref}) - L_{t0_{ref}})$. Here, $L_t(p_{ref})$ is determined, using Eq.(2.4) and a linearly interpolated p_{ref}.
Better results have been obtained with p_{ref} and $F_{t_{ref}}$ as inputs. The feedforward signal $L_{t0_{ref}}$ is found by applying Eq.(3.21). Rest length of tendons now corresponds to the linearly interpolated p_{ref} and $F_{t_{ref}}$. The benefit of this is, that the rest length of the tendons corresponds to the correct reference tension and reference nodal positions *at every time step*. Furthermore, it is more important to guarantee tension in the tendons, than to guarantee a certain rest length. The feedforward control scheme is presented in Figure 5.8. The block $q_{nl} \rightarrow q$ refers to Figure 4.1.

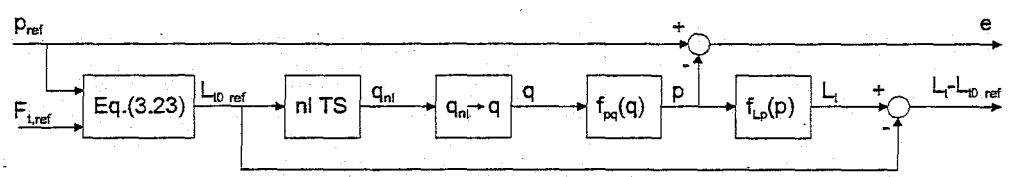

Figure 5.8: Feedforward control scheme of the nonlinear tensegrity structure

Since the 2D tensegrity structure has 15 DOFs, it is decided to choose 15 nodal directions p_{cont} for the description and control of the complete tensegrity structure. The choice for p_{cont} is presented in Eq.(5.2).

$$p_{cont} = \left[p_{1_y}\ p_{3_y}\ p_{4_y}\ p_{5_x}\ p_{5_y}\ p_{6_x}\ p_{6_y}\ p_{7_y}\ p_{8_y}\ p_{9_y}\ p_{10_y}\ p_{11_x}\ p_{11_y}\ p_{12_x}\ p_{12_y}\right]^T \tag{5.2}$$

The controlled nodal positions are chosen by looking at the DOFs per bar. For every DOF one free nodal direction of a node connected to that bar is selected. Since the shape change is mainly vertical, the y-direction of the nodes is preferred over the x-direction.

The error between the reference nodal positions and real nodal positions is presented in Figure 5.9. The first second is used for the shape change, the final half second is used to let the system come to rest. The maximum error between the reference and real positions is never greater than 0.6 mm. However a lot of residual vibrations are present after the shape change is completed.

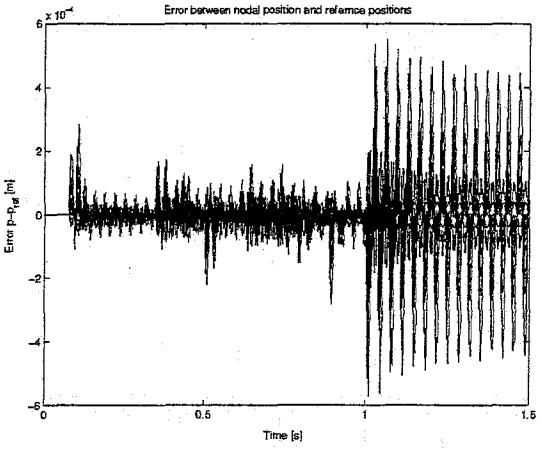

Figure 5.9: Error between p_{cont} and reference nodal positions (y-axis x10^{-4})

In Figure 5.10 the elongations of tendon 1 (connecting nodes 1-2) and tendon 17 (connecting nodes 10-7) are given. When an elongation is negative, no force is applied by that tendon, since the tendons are modelled as one-sided springs. During and after the shape change tendon 1 fluctuates between positive and negative elongations. The negative part corresponds to tendon 1 being slack. Tendon 17 only goes slack after the reference trajectory is ended. In both plots it can be seen, that there are several high frequent vibrations present.

5.2.3 Linearization

Linearization of the nonlinear model has been done using the MAD toolbox [23]. The magnitude plots of four transfer functions of the linearized model are given in Figure 5.11. The magnitude plots present the magnitude from the inputs tendons 1 (node 1-2) and 2 (node 1-5) to the outputs $p_{1_y}\ p_{3_y}$. When these magnitude plots are compared to other

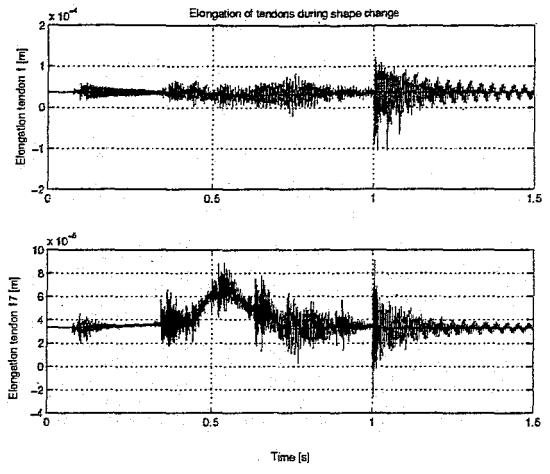

Figure 5.10: Elongation of a) tendon 1 (y-axis x10^{-4}) and b) tendon 17 (y-axis x10^{-5})

magnitude plots in the linear system, it is seen that the first resonance frequencies are approximately the same for all plots, though the position of the first anti-resonance varies between the 15 Hz and 125 Hz. For all transfer functions, between approximately 200 Hz and 1200 Hz there are a number of extra resonances and anti-resonances, and for frequencies larger than 1200 Hz the magnitude decreases with a constant slope.

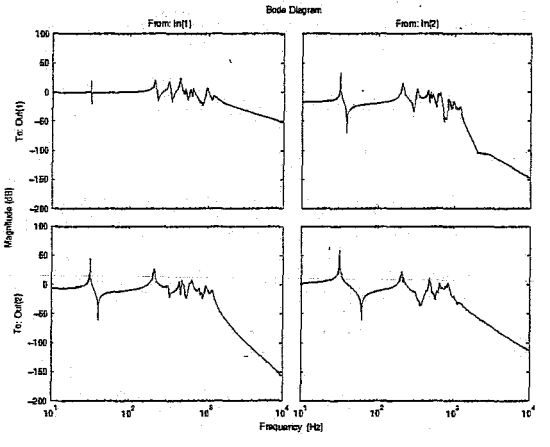

Figure 5.11: Magnitude plot of the linearized tensegrity structure

To compare the nonlinear and the linearized model, a simulation is done. A step change in rest length of tendon 1 is set on both the nonlinear and linearized models. The step of 10^{-5} m is smaller than the smallest elongation of the tendon, so that only the linear part of the nonlinear system is activated. The results for p_{1_y} are presented in Figure 5.12 a). The error between the linearized and nonlinear system is shown in 5.12 c). The error is of order 10^{-9}

and caused by the accuracy of the simulation and rounding errors in the linearization. Since other nodal directions give similar results, it can be concluded that the linearized model is correct.

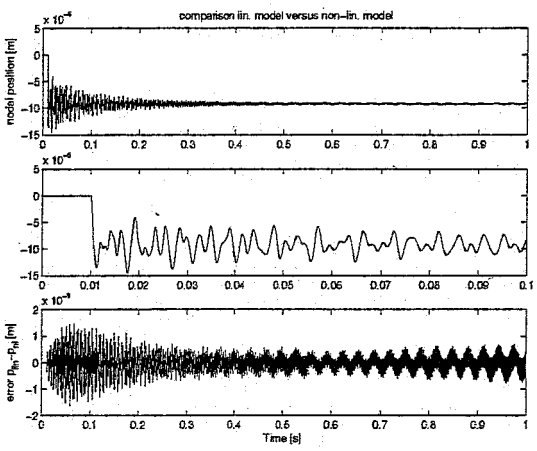

Figure 5.12: a) p_{1_y} of lin. and nonlin. system (y-axis x10^{-6}), b) zoom of a) (y-axis x10^{-6}), c) error $p_{lin} - p_{nl}$ for p_{1_y} (y-axis x10^{-9})

From Figure 5.12 it is seen that the linear and nonlinear model respond equally. This only holds for situations where tendons do not go slack, elongations are not too large, and shapes are not changed too much from an equilibrium situation. As long as a stable feedback controller avoids tendons from going slack, stability of the closed loop is expected for this system.

There are 53 operating points in the shape change. Around each point a linear model can be derived. Gathering the resonance frequencies and dimensionless damping of all the operating points result in Figure 5.13 and 5.14 respectively.

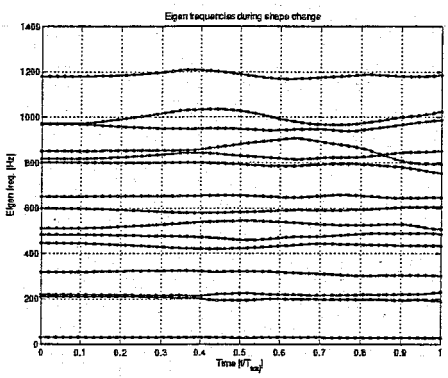

Figure 5.13: Resonance frequencies of linearized models during shape change

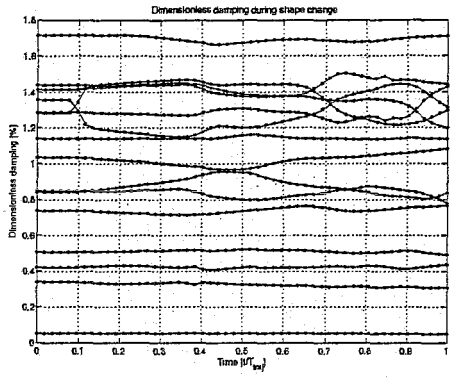

Figure 5.14: Dimensionless damping of linearized models during shape change [%]

The current linearized models have 26 states. If desired, model reduction can simplify the model by reducing the number of states. For every resonance frequency two states should be included into the linear model. In this example the full linearized model is used for the controller design.

5.3 Control

In Section 4.2 it is suggested to design a controller using LMI's. However the calculations turn out to be so extensive that too little computational capacity is available for this approach. When more efficient LMI software is used, there are numerical issues that result in infeasible solutions. The consequence is, that the dual goal of $\mathcal{H}_2$ control together with pole placement cannot be reached. Standard approaches for design of an $\mathcal{H}_2$ controller, i.e., using Riccati equations, will be used instead.

5.3.1 Controller design

With the three objectives described in Subsection 4.2.2, several simulations have been done. These simulations differ in measurement variable p and L_t and in the configuration of the controller (2 DOF controller or 1 DOF controller). In the simulations where the 2 DOF controller is used, $r_{2,ref} = F_{t_{ref}}$ is chosen as second input.
In simulations, variations in the initial values for $q_{nl}(0)$ gave satisfying results for all controllers. Applying a step on a reference signal $p_{i_{ref}}$, again gave good results. However when tracking the reference trajectory, no decent results could be found using L_t as measurement or using a 2 DOF controller. Though no precise explanation has been found, it could be that the linearized mapping from L_t to L_{t_0} (input-output of the controller) changes so much during the shape change, that from the measurements, the controller cannot reconstruct a decent control action anymore. Simulations with the 2 DOF controller show, that the controller does react on errors in the nodal positions, but a relatively large error remains. Partly this can be explained by the fact that there is no pure integrator action present

in the controller. Perhaps a combination of the reference nodal positions, measured nodal positions and reference forces has been found, so that no further control effort has been made to reduce the nodal position errors?
The 1 DOF controller with measurements p_{cont} *has* given promising results. Therefor it is decided to continue the controller design with p as measurement variable and a 1 DOF controller.
What rests is optimizing the controller. This can be done by adjusting the different weighting filters. The input filters are presented in the first plot in Figure 5.15. The second plot in 5.15 shows the output filters. All filtering has been done with first order filters to limit the number of states of the final controller. Static weighting filters do not give a decent representation of the input signals or output objectives, and higher order filters rapidly increase the number of states in the controller.

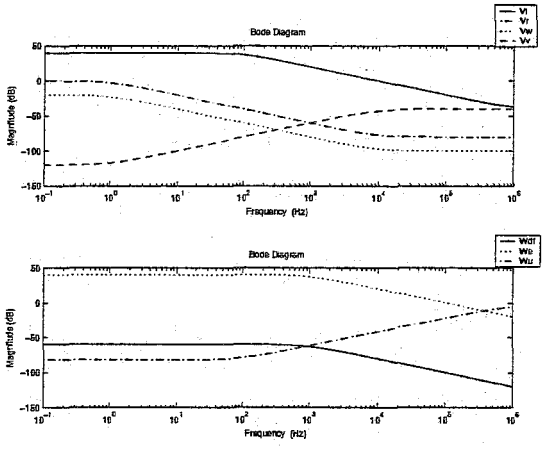

Figure 5.15: Applied weighting filters, used in the $\mathcal{H}_2$ design

The cut-off frequencies of the input filters are chosen to correspond to the spectrum of the input signals. To determine the gains of the filters, the amplitude of the inputs is studied. Variations in p_{ref} are in the order of $O(10^{-1})$. Variations in $F_{t_{ref}}$ are around $O(10)$, for w it is estimated to be $O(10^{-2})$ and v varies with $O(10^{-3})$. Using p_{ref} as reference (by setting its gain to 0 dB), the other amplitudes can simply be obtained.
The cross-over frequencies of the outputs filters have been estimated to include the regions which are important for the different objectives. Looking at the transfer functions from u to the objectives, it turns out that the amplitude of the transfer function from u to ΔF is in the order $O(10^5)$ while the amplitudes from u to p and u are of order $O(1)$. This factor is introduced by the stiffness $EA_t/L_{t_0} \approx 10^5$. Before fine tuning of the output gains can be done, the gain of $W_{\Delta F}$ should be multiplied by 10^{-5} so that all objectives are of the same order.
In the $\mathcal{H}_2$ control design, the control objective of error reduction is in conflict with maintaining tension in the tendons. Larger error reduction will lead to larger control efforts and the possibility that tendons go slack. Preserving the reference tension in the tendons will

result in larger errors. Therefor a compromise must be found between error suppression and tension in the tendons. By looking at position errors and elongation of the tendons in simulations, fine tuning of the gains of the output weighting filters has been done and a compromise has been found.
To reduce the number of states of the controller, pole-zero cancellation has been applied. The state space presentation of the controller is therefor converted to zero-pole-gain form, after which matching poles and zeros are removed. The accuracy of the method is of order $O(\sqrt{\varepsilon})$, with ε the machine accuracy.
The final scheme for the augmented plant is presented in Figure 5.16. Figure 5.17 presents the final closed loop scheme.

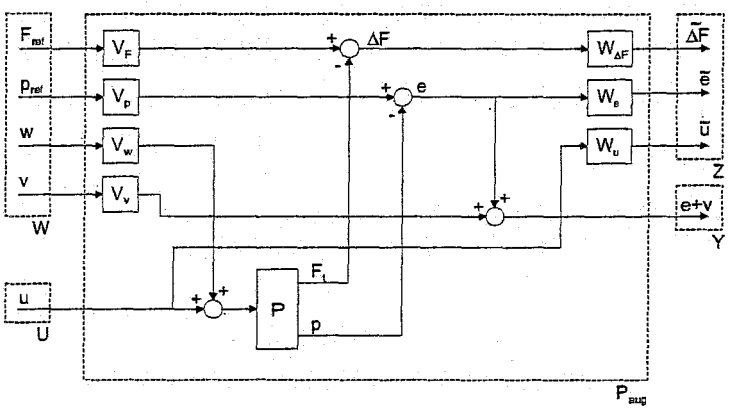

Figure 5.16: Final augmented plant

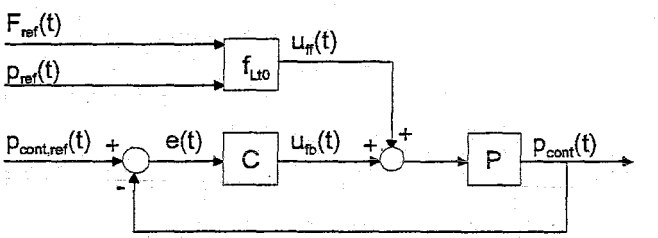

Figure 5.17: Final closed loop scheme

5.3.2 Controller results

The closed loop system including the controller has been checked for stability. At every operating point in the trajectory the closed loop system is stable. When the dimensionless damping of the linearized model is compared to the initial closed loop system, the dimensionless damping for resonance frequencies up to around a 1000 Hz is increased dramatically: from $O(10^{-3})$ to 0.45 and larger. The closed loop eigen frequencies between approximately 1000 Hz and 6000 Hz have damping between $2.3 \cdot 10^{-2}$ and $9.5 \cdot 10^{-2}$, while the linearized

model does not surpass $1.4 \cdot 10^{-2}$. Larger closed loop eigen frequencies have damping equal to or close to 1.
In Figure 5.18 the sensitivity, complementary sensitivity and process sensitivity from the first two inputs to the first two outputs of the corresponding transfer functions are shown. In Appendix B the transfer function of the controller and open loop, the singular value plot of the closed loop system and the step response are presented.

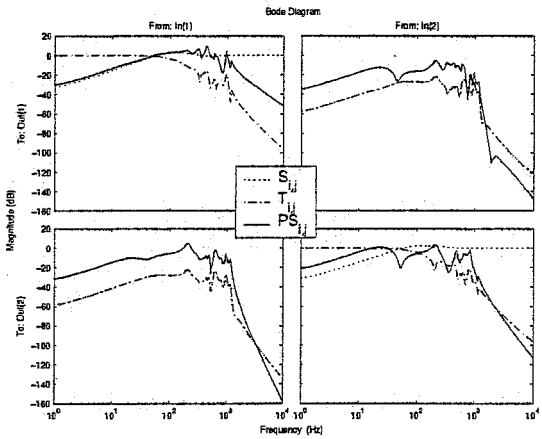

Figure 5.18: Sensitivity S, complementary sensitivity T and Process Sensitivity PS

On the diagonal of Figure 5.18, the sensitivity S has a gain around $-30dB$ for low frequencies. This corresponds to reasonable tracking of the reference signals. For high frequencies the complementary sensitivity T has a low gain. This results in good suppression of the high frequent measurement noise. The cross terms in T are small compared to the diagonal, indicating that control of one nodal position does not have much influence on the position of other nodes. The sensitivity S and process sensitivity PS both have a low gain at low frequencies. This indicates that low frequent disturbances on the output and control effort, for S and PS respectively, are well suppressed. Unfortunately, the cross terms in PS are large as well, indicating possible interference of actuator disturbances with all outputs.

5.3.3 Simulation results

Finally the simulation results are presented. In Figure 5.19 the feedforward position error is compared to the feedback error. Figure 5.20 zooms in on the feedback error from Figure 5.19. The error peaks at $t = 1s$ can be explained by the abrupt stop of the shape change. As can be seen, the residual vibrations die out very quickly. Furthermore, the overall error amplitudes have been reduced.
In Figure 5.21 the elongation of the tendons during and after the shape change is presented. The only time when tendons go slack, is when the trajectory ends (at $t = 1s$). Again this is the result of the abrupt stop of the trajectory. When more attention is paid to the end of the trajectory, e.g., by slowly stopping the shape change, the peaks can be avoided.
Finally the feedback control effort is presented in Figure 5.22.

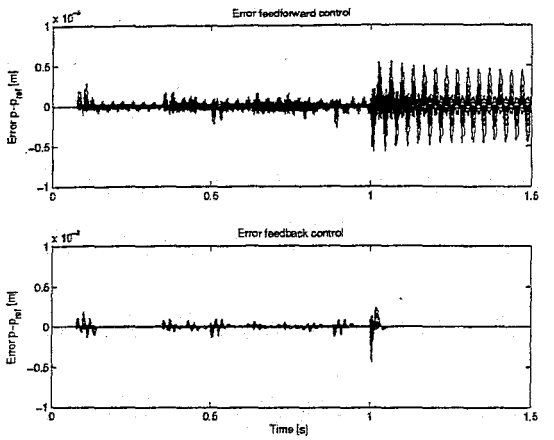

Figure 5.19: Error in nodal directions, a) feedforward error (y-axis x10^{-3}), b) feedback error (y-axis x10^{-3})

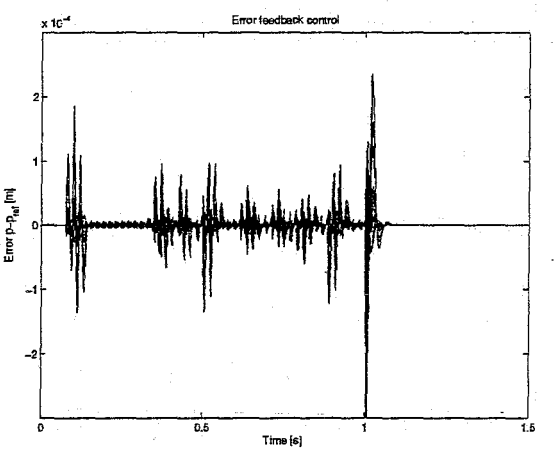

Figure 5.20: Error in nodal directions, zoomed in from 5.19 b) (y-axis x10^{-4})

Note that corrections on the rest length of the tendons by the feedback controller are extremely small ($O(10^{-5})$). This is due to the high stiffness of steel, from which the tendons are made. In the second plot of Figure 5.22 small oscillations can be seen. These are the result of switching to a next operating point. Though linear interpolation is done, switching between operating points leads to discontinuous first derivatives in the linearly interpolated reference signals. If the simulation would be done with p_{ref} and $L_{t_{0_{ref}}}$ the oscillations would be much larger.

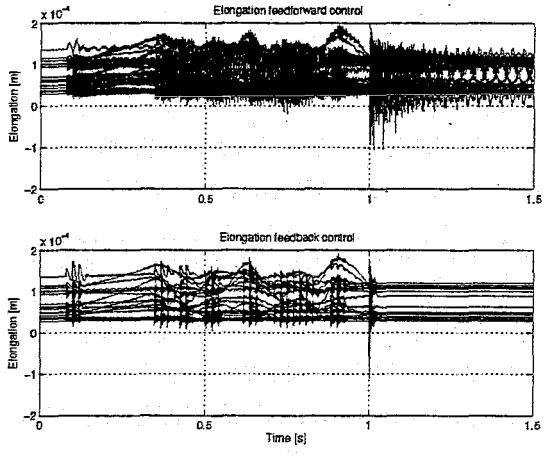

Figure 5.21: a) elongation feedforward control (y-axis x10^{-4}), b) elongation feedback control (y-axis x10^{-4})

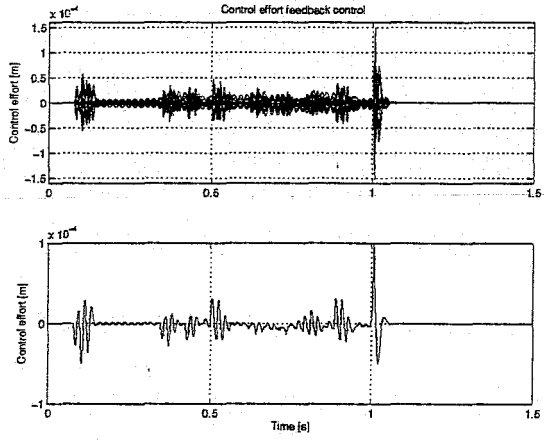

Figure 5.22: a) control effort all tendons (y-axis x10^{-4}), b) control effort tendon 3 (y-axis x10^{-4})

Chapter 6

Conclusions and recommendations

Conclusions

This report has discussed the topics of the design and control of a shape change of a Class 1 tensegrity structure. Initially three important kinematic relations have been presented, together with their characteristics. With multi-body theory a dynamic model for an arbitrary Class 1 tensegrity structure has been derived. To avoid possible singular situations in the dynamics, Euler parameters have been introduced. The extra degrees of freedom introduced by the Euler parameters has been dealt with, so that drift is unlikely to occur. Restrictions on nodal positions, resulting in algebraic relations in the dynamics of the structure, have been removed from the total dynamics of the structure. To guard the integrity of the tensegrity structure, expressions for a stable equilibrium of the system with and without presence of gravity have been derived.

For the design of a reference trajectory several aspects have been studied. Configurations of a tensegrity structure have been tested for singularities and mathematical expressions for (lack of) manipulability have been presented. Furthermore collision of elements has been looked at. This has resulted in an optimization procedure that determines the minimum distance between two elements. Singularity avoidance and collision detection have been the main topics for the design of the reference trajectory, but several geometric and force related conditions have been derived as well. After discussion of possible objectives and optimization variables a reference trajectory generator has been presented. This generator accounts for the different constraints, like collisions and singularities, while minimizing the objective.
The structure of the optimization algorithm for the reference trajectory generator is very simple. If desired, constraints can be added or removed and objectives can be altered, without changing the structure of the algorithm. Of course introducing more, or more stringent, constraints can lead to infeasible trajectories.

To be able to make a decision on which controller to use for the reference trajectory, several control strategies have been studied. The selected control strategy consists of an $\mathcal{H}_2$ controller together with pole placement. Since the selected control strategy requires a linear

system, linearization of the nonlinear model has been done. The extra degrees of freedom from the Euler parameters, resulting in dependency of states in the linearized model, have been removed from the linear model by removing the dependency in the Euler parameters. The linearized model has been verified by comparing simulations of the linearized model with the nonlinear model.
The different aspects related to the design of an $\mathcal{H}_2$ controller have been discussed. This included selection of the measurement variables, inputs, outputs or control objectives, external disturbances and specification of the spectra of the different inputs and outputs.

The original strategy of $\mathcal{H}_2$ control with pole placement turns out to be too computational demanding. To solve this, pole placement has been removed from the control design strategy. A reference trajectory and feedback controller have been designed for a two dimensional Class 1 tensegrity structure. At every operating point of the reference trajectory the linearized *closed loop* system is checked for stability and disturbance suppression, damping and tracking capabilities.
First simulations have been done with only a reference trajectory to simulate feedforward control. This resulted in poorly damped structural vibrations and sometimes in slackness of some tendons. Including the feedback controller reduced the position error and tension in the tendons has been maintained throughout the shape change. Vibrations in the structure have been decreased dramatically.

Both goals of this research, i.e., design of a reference trajectory for an arbitrary Class 1 tensegrity structure and design of a controller with good tracking while maintaining integrity of the structure, have thus been reached. However, since singularity avoidance and collision detection has not been included in the example, no conclusions about these aspects can be drawn.

Recommendations
The first recommendation is related to the assumptions made in this report. These assumptions have been made to simplify the modelling of a tensegrity structure, but it is not clear what the influence of them is on the dynamic behavior of the tensegrity structure. Therefor the different simplifications should be modelled and compared to the model presented in this report or to an experimental testbed. By comparing the old and new situation, conclusions can be drawn about the correctness of the dynamic model.
The dependency of the Euler parameters in the nonlinear dynamics have been removed by rewriting the time derivatives of one Euler parameter as function of the others. For short time spans, simulations gave the impression that this approach is successful. However, no proof for stability is derived nor are the effects of simulation errors for longer time spans studied. If the proposed approach is not suitable, can stability projections resolve the issue of numerical errors, or do Lagrange multipliers give the best results? Are there perhaps other methods that can be used?
The reference trajectory generator includes a constraint for singularity avoidance. Singular situations, however, look closely related to situations where a tensegrity structure looses its integrity. It should be studied if singularities are equivalent to integrity. If they are similar,

the singularity check can be removed from the reference trajectory generator. If not, what are the extra benefits of the singularity check?
Due to the limited amount of time for this research a Gain Scheduling Control strategy has not been implemented. For some or perhaps all shape changes this control strategy could further increase the performance of the closed loop system. Another possibility is the design of a nonlinear controller that guarantees stability and performance, without prior knowledge of the reference trajectory.
After all the simulations it is time to use an experimental testbed for testing. A practical solution for actively changing the rest length of tendons however remains a challenge: the actuator should be able to make relatively large and small changes to the lengths and simultaneously cope with relatively large forces. Possibly a tendon can contain a piezo electrode for small displacements and a linear or rotary motor for larger variations in rest length of the tendon. The motor can be used to handle the feedforward signals, while the piezo electrode can handle the feedback control signals.
Finally a practical recommendation. The theory presented in this report is derived for Class 1 tensegrity structures. To expand the use of the reference generator and the control strategy, theory for Class 2 tensegrity structures should be derived as well. The only items that have to be studied again are the statics for Class 2 tensegrity structures, and the lower and upper bounds in the collision detection.

Bibliography

[1] K. Snelson. *Continuous Tension, Discontinuous Compression Structures.* US Patent 3.169.611, Feb 1965.

[2] K. Snelson. http://www.kennethsnelson.net.

[3] R.E. Skelton and et al. An introduction to the mechanics of tensegrity structures. www.mae.ucsd.edu/research/reskelton/tbook41.pdf, University of California San Diego, 2001.

[4] B. de Jager and R. Skelton. Optimizing stiffness properties of tensegrity structures. In *Proc. of 2001 ASME Int. Mechanical Engineering Congress and Exposition*, New York NY, USA, November 11-16 2001.

[5] B. de Jager, M. Masic, and R. Skelton. Optimal topology and geometry for controllable tensegrity systems. In *IFAC, 15th Triennial World Congress*, Barcelona, Spain, 2002.

[6] C. Sultan and R.E. Skelton. Deployment of tensegrity structures. *Int. Journal of Solids and Structures*, (40):4637–4657, 2003.

[7] J.B. Aldrich, R.E. Skelton, and K. Kreutz-Delgado. Control synthesis for a class of light and agile robotic tensegrity structures. In *Proc. of the American Control Conference*, pages 5245–5251, Denver, Colorado USA, June 4-6 2003.

[8] N. Kanchanasaratool. *Control of Flexible Structure.* PhD thesis, The Australian National University, March 2003.

[9] M.J. van de Molengraft. Dynamics and control of deployable tensegrity structures. Report CST 2002.75, Eindhoven University of Technology, 2002.

[10] H. Baruh. *Analytical Dynamics.* McGraw-Hill, 1999.

[11] J.C.K. Chou. Quaternion kinematic and dynamic differential equations. *IEEE Transactions on Robotics and Automation*, 8(1):53–64, February 1992.

[12] R. Serban and E.J. Haug. Globally independent coordinates for real-time vehicle system simulation. *Journal of Mechanical Design*, 122(4):575–582, 2000.

[13] A.L. Schwab. Quaternions, finite rotation and euler parameters. www.ocp.tudelft.nl/em/staf/schwab/Sch02.pdf, May 16 2002.

[14] H.J. Schek. The force density method for form finding and computation of general networks. *Computer Methods in Applied Mechanics and Engineering*, 3(1):115–134, January 1974.

[15] Tae-Wook Park and Hyun-Seok Yang. A study on singularity avoidance and robust control of redundant robot. In *Proc. 4^{th} world Congress on intelligent control and automation*, pages 1687–1691, Shanghai, China, June 10-14 2002.

[16] John Ting-Yung Wen and L.S. Wilfinger. Kinematic manipulability of general constrained rigid multibody systems. *IEEE Transactions on Robotics and Automation*, 15(3):558–567, June 1999.

[17] C.L. Lewis and A.A. Maciejewski. Fault tolerant operation of kinematically redundant manipulators for locked joint failures. *IEEE Transactions on Robotics and Automation*, 13(4):622–629, August 1997.

[18] K.N. Groom, A.A. Maciejewski, and V. Balakrishnan. Real-time failure-tolerant control of kinematically redundant manipulators. *IEEE Transactions on Robotics and Automation*, 15(6):1109–1116, December 1999.

[19] C. Cocca, D. Cox, and D. Tesar. Failure recovery in redundant serial manipulators using nonlinear programming. Technical report, University of Texas, Austin TX, USA, May 1999.

[20] M. Lin, D. Manocha, J. Cohen, and S. Gottschalk. Collision detection: Algorithms and applications. *Algorithms for Robot Motion and Manipulation*, pages 129–142, 1996.

[21] F. Pfeiffer and C. Glocker. *Multibody Dynamics With Unilateral Contacts*. John Wiley & Sons Inc., 1996.

[22] S. Boyd, L. El Ghaoui, E. Feron, and V. Balakrishnan. *Linear Matrix Inequalities in Systems and Control Theory*. SIAM, Philadelphia, 1994.

[23] S. Forth. *MAD - a Matlab Automatic Differentiation Toolbox*. AMOR report, User guide for MAD, June 2001.

[24] J. Jang, C.S. Ceng, J.A.D. Abreu-Garcia, and Y. Xu. Model reduction of unstable systems. *Int. Journal of System Science*, 24(12):2407–2414, 1993.

[25] B. de Jager and R. Skelton. Input/output selection for planar tensegrity models. In *Proc. of the 40th IEEE Conference on Decision and Control*, pages 4280–4285, Orlando, Florida, USA, December 2001.

Appendix A

Specifications of the 2D tensegrity structure

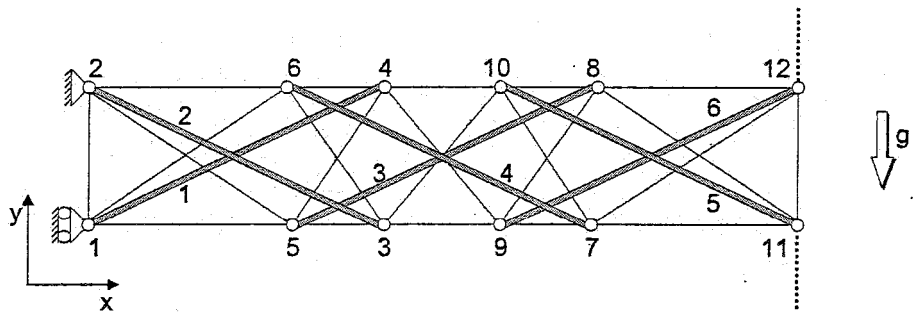

Figure A.1: 2D tensegrity structure

The material used for simulations has the following material and geometric properties:

Table A.1: Material and geometric properties

ρ	$7801\ kg/m^3$
E	$2.07 \cdot 10^{11}\ N/m^2$
σ_{yield}	$4.00 \cdot 10^{8}\ N/m^2$
d_{damp}	$12\ Ns/m$
$r_{b_{in}}$	$7 \cdot 10^{-3}\ m$
$r_{b_{out}}$	$10 \cdot 10^{-3}\ m$
r_t	$1 \cdot 10^{-3}\ m$

The material properties are those of steel, r_i correspond to radii of the bars or tendons.

The nodal positions are:

Table A.2: Node coordinates

$p_1 = [0,\ 0,\ 0]^T$	$p_2 = [0,\ 0.25,\ 0]^T$	$p_3 = [0.5,\ 0,\ 0]^T$
$p_4 = [0.5,\ 0.25,\ 0]^T$	$p_5 = [0.35,\ 0,\ 0]^T$	$p_6 = [0.35,\ 0.25,\ 0]^T$
$p_7 = [0.85,\ 0,\ 0]^T$	$p_8 = [0.85,\ 0.25,\ 0]^T$	$p_9 = [0.7,\ 0,\ 0]^T$
$p_{10} = [0.7,\ 0.25,\ 0]^T$	$p_{11} = [1.2,\ 0,\ 0]^T$	$p_{12} = [1.2,\ 0.25,\ 0]^T$

The connectivity matrices for tendons and bars are:

$$S_t = \begin{bmatrix} 1 & 1 & 2 & 1 & 2 & 5 & 6 & 6 & 5 & 3 & 4 & 3 & 4 & 9 & 10 & 9 & 10 & 7 & 8 & 11 & 7 & 8 \\ 2 & 5 & 6 & 6 & 5 & 3 & 4 & 3 & 4 & 9 & 10 & 10 & 9 & 7 & 8 & 8 & 7 & 11 & 12 & 12 & 12 & 11 \end{bmatrix}^T$$

$$S_b = \begin{bmatrix} 1 & 2 & 5 & 6 & 9 & 10 \\ 4 & 3 & 8 & 7 & 12 & 11 \end{bmatrix}^T$$

Appendix B

Characteristics of the 2D tensegrity structure

In Figure B.1 the magnitude plot of the controller and open loop is presented. At the frequencies presented in the plot, generally the controller can be seen as an integrator, with sometimes a proportional region. At lower frequencies, the magnitude is constant, at higher frequencies the controller looks like a low-pass filter. All transfer functions in this controller can be seen as a lag controller with low pass filtering.
The open loop plots in Figure B.1 are more or less representative for all H_{ol} transfer functions. Most H_{ol} transfer functions have their first resonance around 30 Hz and many eigen frequencies between 200 Hz and 1200 Hz. Under the 200 Hz no clear anti-resonances are visible. The main difference between the H_{ol} transfer functions is the amplitude.

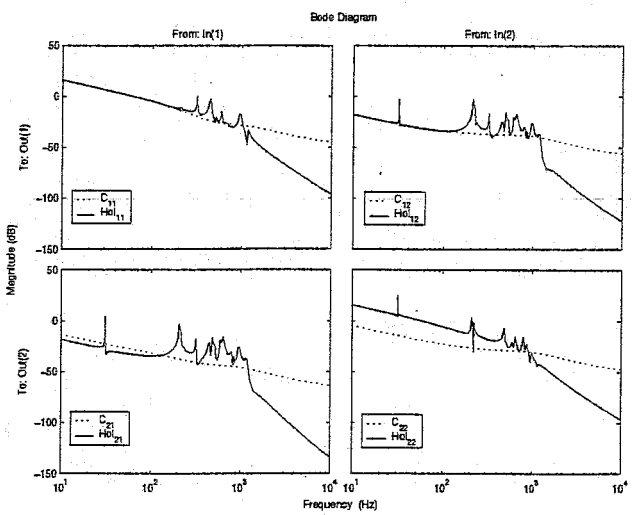

Figure B.1: Feedback controller and open loop magnitude plot

The singular value plot is given in Figure B.2. It is seen that over all frequencies the singular values are not much greater than 0 dB, indicating that the gain between linear combinations of inputs and an output will not be much greater than 0 dB.

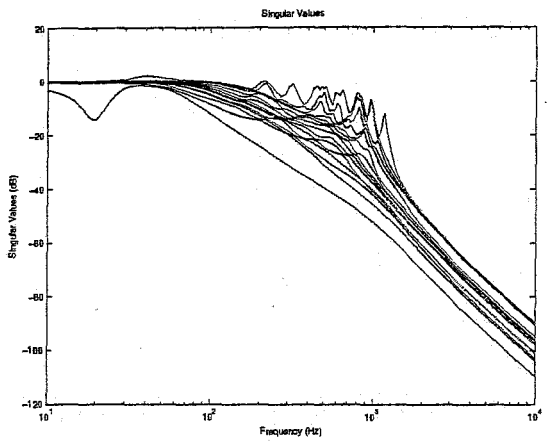

Figure B.2: Singular value plot of the closed loop system

The step response of the closed loop system is illustrated in Figure B.3. There is no non-minimum phase response present in the steps. Some cross terms have a relatively large response (third input to first output, first input to third output), though the greater part of the cross terms are close to zero. The larger outputs correspond to nodal directions that are connected to the same bar as where the step input is applied to. Figure B.3 is representative for the step responses of all inputs.

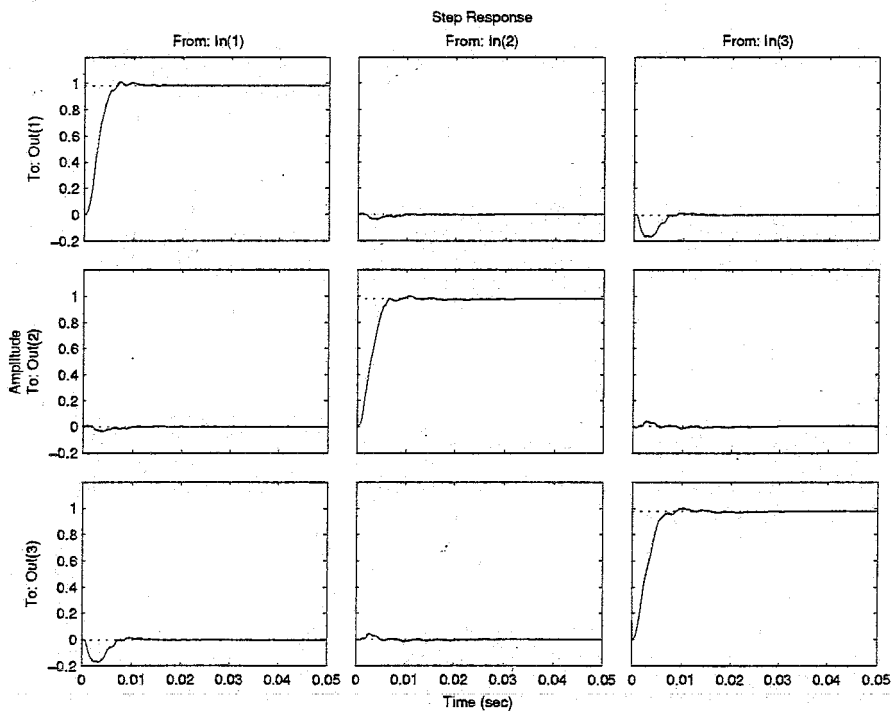

Figure B.3: Step response of the closed loop system